RESEARCH ARTICLE

Robust Sampled-Observer-Based Switching Law for Uncertain Switched Affine Systems Subject to Sensor Faults With an Application to a Bidirectional Buck-Boost DC–DC Converter

DIEGO DOS SANTOS CARNEIRO[1], **FLÁVIO ANDRADE FARIA**[2],
LUCAS JONYS RIBEIRO SILVA[1], **BRUNO MENEGHEL ZILLI**[1],
AND VILMA ALVES DE OLIVEIRA[1], **(Life Senior Member, IEEE)**

[1]Department of Electrical and Computer Engineering, Universidade de São Paulo (USP), São Paulo 13566-590, Brazil
[2]Department of Mathematics, School of Engineering, São Paulo State University (UNESP), São Paulo 15385-000, Brazil

Corresponding author: Vilma Alves de Oliveira (voliveira@usp.br)

ABSTRACT This paper proposes a robust sampled-observer-based fault-tolerant min-type switching law for a class of continuous-time uncertain switched affine systems (SAS) subject to persistent bounded sensor faults using Luenberger observers to estimate the system state. The switching law is designed to make the trajectories of the system be attracted to an open ball containing a given equilibrium point, even in the presence of faults and norm-bounded uncertainties. First, nonlinear matrix conditions are given to obtain the switching law that guarantee the practical stability of a class of uncertain SAS whenever persistent bounded sensor faults are present. To reduce the complexity of the nonlinear matrix conditions, we thus provide LMI-based conditions to obtain the observer gains at the cost of increasing the estimation of the ball for which the trajectories of the system are attracted. Next, we estimate the radius of the open ball by solving a minimization problem using the gains obtained by satisfying the LMI conditions. We then propose an algorithm to search for a set of equilibrium points for a class of uncertain SAS with two system modes, which can be applied to DC–DC converters such as boost, buck, buck-boost, and Cuk converters. Finally, experiments using hardware in the loop of a bidirectional buck-boost DC–DC converter illustrate the efficiency of the fault-tolerant strategy.

INDEX TERMS Switched systems, sampled-data systems, fault-tolerant control, observers, uncertain systems.

I. INTRODUCTION

Persistent bounded sensor faults always produce measurement errors after their occurrence, and the faults continue to exist until the faulty component is fixed or replaced [1].

The associate editor coordinating the review of this manuscript and approving it for publication was Mark Kok Yew Ng.

For switched systems such as DC microgrids, sensor faults can also be a result of a typical attack known as a false-data injection attack. In this event, a malicious entity injects a false signal in the measurement (sensors) or communicated signal, which can lead the microgrid to instability [2], [3].

Moreover, the presence of persistent sensor faults together with uncertainties can adversely affect the performance and

reliability of a control system, and a desired equilibrium point may not be achieved, particularly when any output feedback is applied, including static output feedback and observer-based strategies.

In the context of generating a min-type switching law to make the trajectories of a continuous-time switched affine systems (SAS) be attracted to an equilibrium point when not all state variables are available for measurement, [4] proposed an observer-based min-type switching law for a class of SAS to guarantee the asymptotic stability of a given equilibrium point in a known family. However, in [4], uncertainties and sensor faults were not considered in the observer and switching law design. On the other hand, [5] and [6], proposed a robust observer-based switching law strategy for a class of uncertain SAS, whereas in [7] and recent works [6], [8], an observer-based switching law for a class of SAS under bounded disturbances in the dynamics ([7], [8]) as well as in the output ([6]) was proposed.

The aforementioned approaches do not consider sensor faults in the switching law design, although the strategy proposed in [6] can be adapted to a fault-tolerant switching law if the output disturbances are considered as persistent bounded sensor faults. In addition, there are few works in the literature that propose a fault-tolerant strategy for SAS or uncertain SAS to accommodate sensor faults if all sensors are prone to faults and not all state variables are available for measurement.

For instance, [9] and [10] proposed a fault accommodation strategy through system reconfiguration. However, fault detection and isolation were required. In addition, the authors assumed that not all sensors were simultaneously subject to a fault, and robustness against uncertainties was not considered.

Moreover, when fault detection is considered, recent works such as [11] and [12] proposed data-driven methods to enhance the reliability of power electronic systems. However, it is still necessary to provide a fault-tolerant switching law for a critical scenario in which all sensor faults occur at the same time.

Furthermore, the frequency limitations of switching devices in practice can also affect the stability properties of switched systems when a min-type switching law is considered. For instance, the switching frequency for silicon-made IGBT switching devices is approximately 6 to 10 kHz, whereas for silicon-carbide MOSFET, it is approximately 10 to 35 kHz [13]. Hence, to avoid the chattering/Zeno phenomenon, the switching frequency generated by the switching law must not be greater than these frequencies.

A min-type switching law with a finite number of switchings in a given time interval can be obtained by guaranteeing dwell-time properties as in [14], [15], [16], and [17], an average dwell-time (ADT) [18], [19], [20] or mode-dependent ADT [21], [22], [23], and [6]. In addition, the practical stability of an uncertain SAS can be achieved by considering a discrete approximation of the system to generate the switching law, as presented in [24], [25],

and [26]. Practical stability can also include performance indices in control design as in [6] and [23].

Another alternative to avoid high-frequency switching is a sampled-based approach, as in [27] for uncertain SAS under polytopic uncertainties. However, the presented solution assumed that the state is available for measurement, and sensor failures were not considered. On the other hand, [8], [28], and [6] proposed a switching law strategy considering a robust sampling-based switching law with robustness against persistent disturbances for switched affine systems. However, [28] considered all state variables available for measurement, and in [6], [8] and [28] the analysis of the matrices of the gain obtained was for a given equilibrium point without addressing uncertainties and sensor failures.

In [29], two different strategies were provided to obtain the switching law and observer gains for uncertain SAS. However, the gains were obtained without considering the frequency limitation of the switching device (although the authors mentioned that for practical application, the switching frequency must be constrained), and fault tolerance was not taken into consideration. However, Theorems 1 and 2 in [29] guarantee that the trajectories of the uncertain SAS converge to a region that contains a given equilibrium point in a family in which the pairs of states and outputs are observable, which may not be possible in some practical applications.

In addition, the strategies presented so far guarantee stability, but most of them do not consider fault tolerance to sensor faults and do not provide a solution to an optimization problem. Therefore, the gains obtained cannot guarantee the smallest possible region of attraction within a given upper bound under bounded sensor faults. Moreover, when all sensors are faulty, classical output feedback strategies such as PI control that are not designed to be fault-tolerant can produce extremely high or low values in the state variables that may damage the switched affine system.

In this paper, we propose a robust sampled-observer-based fault-tolerant switching law using samples of the estimated state of a class of uncertain SAS subject to persistent sensor faults when only the output measurements are available and all sensors are prone to faults. The faults are considered to be additive and not state-dependent, representing an offset signal added to the output. A switched Luenberger observer generates the estimation of the system state, and the switching law guarantees that the trajectories of the uncertain SAS are attracted to an open ball containing a given equilibrium point, even in the presence of bounded sensor faults and norm-bounded uncertainties. The observer and switching law gains are obtained by solving an LMI-based optimization problem. The main contributions of this paper can be summarized as follows:

- Design of a switching law for a class of uncertain SAS subject to persistent bounded sensor faults when all sensors are prone to faults, and the system state is not fully available for measurements.

- The proposed fault-tolerant strategy guarantees practical stability even if an offset sensor fault is detected in all sensors as long as the fault magnitudes are within a bound given by the designer. In addition, practical stability is not affected by bounded offset sensor faults caused by cyber-attacks if the fault magnitude is less than the bound given by the designer.
- Considering the limitation on the switching frequency of buck-boost DC–DC converters under load variations and persistent bounded sensor faults, practical stability is also guaranteed and The observer gains and switching law are designed to guarantee optimal robustness against uncertainties and sensor faults.
- For the particular case of DC–DC converters such as buck, boost, buck-boost, and Cuk converters, an algorithm is developed to search for a subset of equilibrium points in a given family such that the trajectories of a class of uncertain SAS are attracted to an open ball with a radius determined by solving an optimization problem based on LMIs.

Furthermore, we remark that the fault-tolerant strategy is novel in the literature since we consider a critical scenario of generating a min-type switching law with limited switching frequency for a class of uncertain switched affine systems under bounded faults in all sensors.

The remainder of this paper is organized as follows. In Sections II and III, we present the mathematical results and definitions from the literature that support the results proposed in this paper. Section IV presents the methodology used to obtain the observer gains and the gains for the switching law. In Section V, we present experimental results for the proposed strategy and its application to a bidirectional buck-boost DC–DC converter. Finally, Section VI presents concluding remarks and directions for future research.

Notation: The symbol $\star$ denotes the transposed element in symmetric matrices, and $(')$ indicates the transpose of vectors and matrices. Negative and positive definite matrices are denoted by $M \prec 0$ and $M \succ 0$, respectively. The sum of matrices is abbreviated as $\text{He}(\mathbf{M}) := (\mathbf{M} + \mathbf{M}')$. The maximum and minimum eigenvalues of a symmetric matrix $\mathbf{M}$ are denoted as $\lambda_{\max}(\mathbf{M})$ and $\lambda_{\min}(\mathbf{M})$, respectively. The set composed of the first M positive integers is denoted as $\mathbb{M}$, where M is the number of system modes. If $\mathbf{M}$ belongs to a set $\{\mathbf{M}_1, \mathbf{M}_2, \cdots, \mathbf{M}_i, \mathbf{M}_M\}$, then $\overline{\lambda}_{\max}(\mathbf{M}) := \max_{i \in \mathbb{M}}(\lambda_{\max}(\mathbf{M_i}))$ and $\underline{\lambda}_{\min}(\mathbf{M}) := \min_{i \in \mathbb{M}}\lambda_{\min}(\mathbf{M_i})$. The set of real positive numbers is denoted by $\mathbb{R}_+$. The convex combination of a set of matrices $\{A_1, \ldots, A_M\}$ is denoted by $A(\kappa) = \sum_{i=1}^{M} \kappa_i A_i$ and the convex combination of a set of vectors $\{g_1, \ldots, g_M\}$ is denoted by $g(\kappa) = \sum_{i=1}^{M} \kappa_i g_i$, where $\kappa = [\kappa_1 \ \kappa_2 \ \cdots \ \kappa_M]'$ belongs to set $\mathbb{K}$ composed of vectors with non-negative components κ_i such that $\sum_{j=1}^{M} \kappa_i = 1$. The set of locally essentially bounded measurable functions $f : \mathbb{R}_+ \to \mathbb{R}^n$ is denoted by $\mathcal{L}_\infty$, and $\|f\|$ is the Euclidean norm. The null space (or kernel) of $\mathbf{M}$ is defined as $\text{Null}(\mathbf{M})$.

II. PRELIMINARIES

The following properties, definitions, and lemmas are required for the main results of this paper.

Property 1: For any positive definite matrix P, we have $\lambda_{\min}(P)I \preceq P \preceq \lambda_{\max}(P)I$.

Lemma 1 [30]: For any matrices M, N of appropriate dimensions and a time-varying matrix $\mathcal{F}(t)$ satisfying $\mathcal{F}(t)'\mathcal{F}(t) \preceq I$, $\forall t \geq 0$, there exists a constant $\varepsilon > 0$ such that $M'\mathcal{F}(t)N + N'\mathcal{F}'(t)M \preceq \varepsilon^{-1}M'M + \varepsilon N'N$.

Lemma 2 (Non-Strict Projection Lemma [31]): Consider $\mathcal{G} \in \mathbb{R}^{m \times n}$, $\mathcal{H} \in \mathbb{R}^{p \times n}$ and Hermitian matrix $\Psi \in \mathbb{R}^{n \times n}$. Let N_G, N_H be the right orthogonal complements of $\mathcal{G}, \mathcal{H}$, respectively. If $N_G'\Psi N_G \preceq 0$ and $N_H'\Psi N_H \preceq 0$ then, there exists $V \in \mathbb{R}^{p \times m}$ such that $\Psi + \mathcal{G}'V'\mathcal{H} + \mathcal{H}'V\mathcal{G} \preceq 0$.

III. PROBLEM FORMULATION

We consider the following class of continuous-time uncertain SAS subject to persistent bounded sensor faults and under norm-bounded uncertainties[1]:

$$\dot{x} = (A_\sigma + \Delta A_\sigma)x + b_\sigma, \quad x(0) = x_0$$
$$y = C_\sigma x + F_\sigma f_s, \quad (1)$$

where $x \in \mathbb{R}^n$ is the state, $y \in \mathbb{R}^p$ is the output, $f_s \in \mathcal{L}_\infty^p$ is the sensors faults vector, with $p < n$, $\sigma : \mathbb{R}^M \to \mathbb{M}$ is a sampled-data based switching law that selects a known mode i among M available ones in set $\mathbb{M}$ at each sampled instant $0 = t_0 < t_1 < \cdots < t_k < \cdots$, with $\lim_{k \to \infty} t_k = \infty$. The matrices $A_i \in \mathbb{R}^{n \times n}$, $b_i \in^{n \times m}$, $C_i \in \mathbb{R}^{p \times n}$ and $F_i \in \mathbb{R}^{p \times p}$, $i \in \mathbb{M}$, represent the state, input, output and fault distribution matrices, respectively. The uncertainty matrices ΔA_i have the following form [32]:

$$\Delta A_i = \tilde{\delta}_i Q_i, \quad |\tilde{\delta}_i| \leq 1, \ \forall i \in \mathbb{M}, \quad (2)$$

where $Q_i := M_i N_i$ are given for all $i \in \mathbb{M}$, and $\tilde{\delta}_i : \mathbb{R} \to [-1, 1]$ are defined as unknown functions. The matrices $M_i \in \mathbb{R}^{n \times m_A}$, $N_i \in \mathbb{R}^{m_A \times n}$, with $m_A = \max_{i \in \mathbb{M}}(\text{rank}(Q_i))$, $\forall i \in \mathbb{M}$ are matrices that represent structured uncertainties and are obtained using full rank factorization [33]. In addition, we consider the following assumptions.

Assumption 1: The system state in (1) is not fully available for measurement.

Assumption 2: All sensors are prone to fault, $\text{rank}(F_i) = p$, $\forall i \in \mathbb{M}$ and for a known parameter β_f, we have

$$\|f_s\| \leq \beta_f, \quad 0 < \beta_f < \infty, \ \forall t \geq 0. \quad (3)$$

Assumption 3: The sampled interval $T_k := t_{k+1} - t_k > 0$ can be varying and be less than a known maximum length of the sampled interval defined as $T_{\max}$.

Let x_e be an equilibrium point in a family given as follows

$$\mathcal{X}_e = \left\{x_e \in \mathbb{R}^n : A(\kappa)x_e + b(\kappa) = 0, \forall \kappa \in \mathbb{K}\right\}. \quad (4)$$

---

[1]For some switched power electronic systems representation, the vector b_σ in (1) can be represented as $b_\sigma = B_\sigma u(t)$, where $u \in \mathbb{R}$ is an external input assumed to be constant for all $t \geq 0$ and B_σ is an input matrix. Since u is constant, then b_σ is an affine term.

The stability of (1) is investigated by translating the origin of system (1) to the equilibrium point. Let $\xi := x - x_e$, and $y_\xi := y - C_\sigma x_e$ be the translated state and output vectors, respectively. Then, system (1) can be rewritten as

$$\dot{\xi} = (A_\sigma + \Delta A_\sigma)\xi + g_\sigma + \Delta A_\sigma x_e,$$
$$y_\xi = C_\sigma \xi + F_\sigma f_s, \tag{5}$$

with $g_\sigma = A_\sigma x_e + b_\sigma$. An equilibrium point x_e in family (4) is reached if $\sigma(x(t))$ is continuous for all $t \geq 0$ or if the sampled interval T_k is very small, considering system (5) without uncertainties. In addition, from Assumption 1, we must estimate the state x if a state-feedback switching law is applied. Hence, let $\hat{x}$ be an estimative of x in (1) such that $\dot{\hat{x}} = A_\sigma \hat{\xi} - L_\sigma(y - C_\sigma \hat{x})$, $\hat{x}(0) = \hat{x}_0$, where L_i, $i \in \mathbb{M}$, are the gains of the observer to be designed. In addition, let $\hat{\xi} := \hat{x} - x_e$ be an estimate of ξ in (5), $\hat{y}_\xi := C_\sigma \hat{\xi}$ be the observer output, and let $e = \xi - \hat{\xi} = \hat{x} - x$ be the estimation error. The estimation error and observer dynamics are expressed as follows

$$\dot{e} = (A_\sigma + L_\sigma C_\sigma + \Delta A_\sigma)e + L_\sigma F_\sigma f_s + \Delta A_\sigma(\hat{\xi} + x_e),$$
$$\dot{\hat{\xi}} = A_\sigma \hat{\xi} + g_\sigma - L_\sigma(C_\sigma e + F_\sigma f_s). \tag{6}$$

Next, an augmented system with the observer and estimation error dynamics is defined as

$$\dot{\zeta} = \overline{A}_\sigma \zeta + \overline{F}_\sigma f_s + \overline{C}_\sigma, \tag{7}$$

with $\zeta := \begin{bmatrix} e' & \hat{\xi}' \end{bmatrix}'$, $\overline{C}_\sigma = \begin{bmatrix} (\Delta A_\sigma x_e)' & (A_\sigma x_e + b_\sigma)' \end{bmatrix}'$, and

$$\overline{A}_\sigma = \begin{bmatrix} A_\sigma + \Delta A_\sigma + L_\sigma C_\sigma & \Delta A_\sigma \\ -L_\sigma C_\sigma & A_\sigma \end{bmatrix}, \quad \overline{F}_\sigma = \begin{bmatrix} L_\sigma F_\sigma \\ -L_\sigma F_\sigma \end{bmatrix}.$$

In this paper, we find the observer gains L_i, $i \in \mathbb{M}$, and a positive definite matrix $P \in \mathbb{R}^{n \times n}$ to guarantee the practical stability of system (7), and also make the trajectories of system (1) be attracted to the open ball

$$\mathcal{B}(x_e, \omega) := \{x \in \mathbb{R}^n : \|x - x_e\|^2 < \omega^2\} \tag{8}$$

where $0 \leq \omega < \infty$, when the switching law

$$\sigma(\hat{\xi}_k) = \min_{i \in \mathbb{M}}\left(\arg \min_{i \in \mathbb{M}}\left(\hat{\xi}_k' P(A_i \hat{\xi}_k + g_i)\right)\right), \tag{9}$$

is considered, whenever (2) and (3) hold, where $\hat{x}_k = \hat{x}(t_k)$, $\hat{\xi}_k := \hat{\xi}(t_k)$ and $e_k := e(t_k)$. A diagram of the proposed strategy is shown in Figure 1.

Furthermore, we propose an algorithm to search for a subset of equilibrium points of the family of points $\mathcal{X}_e$ given by (4) such that $x \in \mathcal{B}(x_e, \omega)$ when $t \to \infty$ for a special case when the number of system modes $M = 2$.

Remark 1: The sampled instants t_k in switching law (9) are related to the maximum switching frequency of the switching device, where the maximum switching frequency, denoted as f_{sw}, is given by $f_{sw}(t_k) = 1/t_k$. If the sampled instants are uniform, such that $t_{k+1} - t_k = T_k = T \leq T_{\max}, \forall k > 0$, then the maximum switching frequency satisfies $f_{sw}(t_k) = f_{sw}(T) = 1/T, \forall k > 0$ and the minimum
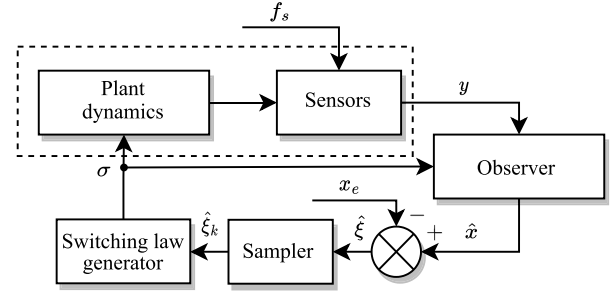

FIGURE 1. Proposed strategy diagram.

switching frequency is $1/T_{\max}$. Thus, by applying switching law (9) in system (1) with a given sampled time $T \leq T_{\max}$, we guarantee that the switching device does not switch more than once between sampled instants, although the opposite is not necessarily true. In other words, the switching device may not switch during a period greater than the sampled period since index i changes according to the error between the current state and the desired equilibrium point, according to the logic given in (9). Thus, the frequency limitation imposed by the sampling strategy allows the practical application of switching law (9), in which the switching device has a limited operational frequency, with the benefit of switching the system modes according to a desired equilibrium point.

IV. MAIN RESULTS

This section presents sufficient conditions in terms of LMIs to obtain a switching law that guarantees the practical stability of (7), whereas the trajectories of (1) are attracted to $\mathcal{B}(x_e, \omega)$ in (8) for a given $x_e \in \mathcal{X}_e$ and for β_f that satisfies (3). In the sequence, we present an algorithm to obtain a set of equilibrium points in family (4) that satisfy (8).

Inspired by [8], to address the problem of determining the observer gains and switching law matrices, we propose the following optimization problem.

Theorem 1: Given $\kappa \in \mathbb{K}$, $x_e \in \mathcal{X}_e$ satisfying (4), $\eta > 0$ and a maximum sample time $T_{\max} > 0$, if there exist positive definite matrices $P \in \mathbb{R}^{n \times n}$, $U_i \in \mathbb{R}^{n \times n}$, matrices $L_i \in \mathbb{R}^{n \times p}$ and positive parameters $\tilde{\varepsilon}_i, \varepsilon_i, \vartheta_i, \gamma_i, \alpha$, solution to the optimization problem (11)-(14), for all $(\sigma(t_k) = i, \sigma(t_k^-) = j) \in \mathbb{M} \times \mathbb{M}$, $i \neq j$, then, the practical stability of system (7) under the sampled observer-based switching law given in (9) is guaranteed, and the trajectories are attracted to

$$\Omega = \{\zeta \in \mathbb{R}^{2n} : \zeta' \mathscr{P} \zeta < \alpha T_{\max}\} \tag{10}$$

where $\mathscr{P} := \text{diag}([P\ P])$. Furthermore, the trajectories of (1) are attracted to (8) with the minimum radius ω.

$$\min_{P, L_i, U_i, \gamma_i, \tilde{\varepsilon}_i, \varepsilon_i, \vartheta_i, \alpha} \alpha, \tag{11}$$

$$\text{subject to: } \mathcal{M}_i(0, 0) \preceq 0 \tag{12}$$

$$\mathcal{M}_i(T_{\max}, T_{\max}^2) \preceq 0 \tag{13}$$

$$\alpha \eta T_{\max} - \vartheta_i T_{\max} - \gamma_i \beta_f^2 > 0 \tag{14}$$

where $\mathcal{M}_i(0, 0)$, $\mathcal{M}_i(T_{\max}, T_{\max}^2)$ are defined by making $\tau = 0$ in (15), as shown at the bottom of the next page, and $\tau = T_{max}$ in (16), as shown at the bottom of the next page, respectively.

Proof: Assume that $\sigma(\hat{\xi}_k) = i$ and choose a Lyapunov-Krasowskii functional given as follows

$$\tilde{V}(\zeta(t), w(t)) = V(\zeta(t)) + w(t) \tag{17}$$

where

$$V(\zeta(t)) = \zeta'\mathscr{P}\zeta = e'Pe + \hat{\xi}'P\hat{\xi} \tag{18}$$

$$w(t) = (t_{k+1} - t) \int_{t_k}^{t} e^{-\eta(t-s)} \dot{e}(s)'U_i\dot{e}(s)ds$$

$$+ (t_{k+1} - t) \int_{t_k}^{t} e^{-\eta(t-s)} \dot{\hat{\xi}}(s)'U_i\dot{\hat{\xi}}(s)ds \tag{19}$$

We aim to show that the following inequality holds:

$$\dot{\tilde{V}} + \eta\tilde{V} = \dot{V} + \eta V + \dot{w} + \eta w \leq \alpha\eta T_{\max}. \tag{20}$$

We denote $\hat{\varphi}(t) = (\hat{\xi}(t) - \hat{\xi}_k)\tau(t)^{-1}$, $\varphi(t) = (e(t) - e_k)\tau(t)^{-1}$, where $\tau(t) := t - t_k$ for all $t \in [t_k, t_{k+1})$. Using the Jensen inequality in (20) with $t_{k+1} - t = T_k - \tau$ and $0 < T_k \leq T_{\max}$, we obtain $\dot{w} + \eta w_i \leq (T_{\max} - \tau)(\dot{\hat{\xi}}'U_i\dot{\hat{\xi}}) - \tau\hat{\varphi}'U_i\hat{\varphi}e^{-\eta T_{\max}} + (T_{\max} - \tau)\dot{e}'U_i\dot{e} - \tau\varphi'U_i\varphi e^{-\eta T_{\max}}$, which corresponds to

$$\dot{w} \leq -\eta w - \tau(\hat{\varphi}'U_i\hat{\varphi} + \varphi'U_i\varphi)e^{-\eta T_{\max}}$$

$$+ (T_{\max} - \tau)\Big(\hat{\xi}'A_i'U_iA_i\hat{\xi} + 2\hat{\xi}'A_i'U_ig_i$$

$$- 2\hat{\xi}'A_i'U_iL_iC_ie - 2\hat{\xi}'A_i'U_iL_iF_if_s + g_i'U_ig_i$$

$$- 2g_i'U_iL_iC_ie - 2g_i'U_iL_iF_if_s + 4e'C_i'L_i'U_iL_iF_if_s$$

$$+ 2f_s'F_i'L_i'U_iL_iF_if_s + 2f_s'F_i'L_i'U_i\Delta A_i(\hat{\xi} + x_e)$$

$$+ e'\big(\mathrm{He}(A_i + L_iC_i)'U_i(A_i + L_iC_i + \Delta A_i))\big)e$$

$$+ 2e'((A_i + \Delta A_i)'U_iL_iF_i)f_s + e'(\Delta A_iU_i\Delta A_i)e$$

$$+ 2e'(\Delta A_iU_i\Delta A_i)\xi + 2e'(\Delta A_iU_i\Delta A_i)x_e$$

$$+ 2e'((A_i' + C_i'L_i')U_i\Delta A_i)(\hat{\xi} + x_e)\Big) \tag{21}$$

$$= -\eta w - \tau(\hat{\varphi}'U_i\hat{\varphi} + \varphi'U_i\varphi)e^{-\eta T_{\max}}$$

$$+ (T_{\max} - \tau)\Big(\hat{\xi}'A_i'U_iA_i\hat{\xi} + 2\hat{\xi}'A_i'U_ig_i$$

$$- 2\hat{\xi}'A_i'U_iL_iC_ie - 2\hat{\xi}'A_i'U_iL_iF_if_s + g_i'U_ig_i$$

$$- 2g_i'U_iL_iC_ie - 2g_i'U_iL_iF_if_s + 4e'C_i'L_i'U_iL_iF_if_s$$

$$+ 2f_s'F_i'L_i'U_iL_iF_if_s + 2f_s'F_i'L_i'U_i\Delta A_i(\hat{\xi} + x_e)$$

$$+ e'\big(\mathrm{He}(A_i + L_iC_i)'U_i(A_i + L_iC_i + \Delta A_i))\big)e$$

$$+ 2e'((A_i + \Delta A_i)'U_iL_iF_i)f_s + \zeta_1'\tilde{\delta}_i^2\tilde{Q}_i\zeta_1$$

$$+ 2e'((A_i' + C_i'L_i')U_i\Delta A_i)(\hat{\xi} + x_e)\Big) \tag{22}$$

where the equality in (22) is obtained by considering the definition of ΔA_i in (2), with $\zeta_1' := \big[e' \ \hat{\xi}' \ x_e' \big]$, and

$$\tilde{Q}_i = \begin{bmatrix} Q_i'U_iQ_i & Q_i'U_iQ_i & Q_i'U_iQ_i \\ \star & Q_i'U_iQ_i & Q_i'U_iQ_i \\ \star & \star & Q_i'U_iQ_i \end{bmatrix}.$$

Since $|\tilde{\delta}_i| \leq 1$, we obtain $\zeta_1'\tilde{\delta}_i^2\bar{Q}_i\zeta_1 \leq \zeta_1'\bar{Q}_i\zeta_1, \forall i \in \mathbb{M}$. Applying Lemma 1 in the remaining uncertain terms of (22), the following inequality is satisfied

$$0 \geq -\tilde{\zeta}\big(\mathcal{U}_i(\tau) + (T_{\max} - \tau)(\varepsilon_i^{-1}\tilde{M}_i'\tilde{M}_i + \varepsilon_i\tilde{N}_i'\tilde{N}_i)\big)\tilde{\zeta}$$

$$+ \dot{w} + \eta w - \vartheta_iT_{\max} \tag{23}$$

where $\tilde{\zeta} := \big[e' \ \hat{\xi}' \ 1 \ f_s' \ \hat{\varphi}' \ \varphi'\big]'$, $\tilde{N}_i = [N_i \ N_i \ N_ix_e \ 0 \ 0 \ 0]$, $\tilde{M}_i = \big[M_i'U_i(A_i + L_iC_i) \ 0 \ 0 \ M_i'U_iL_iF_i \ 0 \ 0 \big]$ and $\mathcal{U}(\tau)$ is given by

$$\mathcal{U}_i(\tau) = \begin{bmatrix} \mathcal{U}_{11}^i(\tau) & \mathcal{U}_{12}^i(\tau) & \mathcal{U}_{13}^i(\tau) & \mathcal{U}_{14}^i(\tau) & 0 & 0 \\ \star & \mathcal{U}_{22}^i(\tau) & \mathcal{U}_{23}^i(\tau) & \mathcal{U}_{24}^i(\tau) & 0 & 0 \\ \star & \star & \mathcal{U}_{33}^i(\tau) & \mathcal{U}_{34}^i(\tau) & 0 & 0 \\ \star & \star & \star & \mathcal{U}_{44}^i(\tau) & 0 & 0 \\ \star & \star & \star & \star & \mathcal{U}_{55}^i(\tau) & 0 \\ \star & \star & \star & \star & \star & \mathcal{U}_{66}^i(\tau) \end{bmatrix},$$

with $\mathcal{U}_{55}^i(\tau) = -\tau U_ie^{-\eta T_{\max}}$, $\mathcal{U}_{66}^i(\tau) = -\tau U_ie^{-\eta T_{\max}}$, and

$$\mathcal{U}_{11}^i(\tau) = (T_{\max} - \tau)\big((A_i' + C_i'L_i')U_iA_i + A_i'U_iL_iC_i$$

$$+ 2C_i'L_i'U_iL_iC_i + Q_i'U_iQ_i\big)$$

$$\mathcal{U}_{12}^i(\tau) = (T_{\max} - \tau)\big(- C_i'L_i'U_iA_i + Q_i'U_iQ_i\big)$$

$$\mathcal{U}_{13}^i(\tau) = (T_{\max} - \tau)\big(- C_i'L_i'U_ig_i + Q_i'U_iQ_ix_e\big)$$

$$\mathcal{U}_{14}^i(\tau) = (T_{\max} - \tau)\big(2C_i'L_i'U_iL_iF_i + A_i'U_iL_iF_i\big)$$

$$\mathcal{U}_{22}^i(\tau) = (T_{\max} - \tau)\big(A_i'U_iA_i + Q_i'U_iQ_i\big)$$

$$\mathcal{U}_{23}^i(\tau) = (T_{\max} - \tau)\big(A_i'U_ig_i + Q_i'U_iQ_ix_e\big)$$

$$\mathcal{U}_{24}^i(\tau) = (T_{\max} - \tau)(-A_i'U_iL_iF_i)$$

$$\mathcal{U}_{33}^i(\tau) = -\vartheta_iT_{\max} + (T_{\max} - \tau)\big(g_i'U_ig_i$$

$$+ x_e'Q_i'U_iQ_ix_e\big)$$

$$\mathcal{U}_{34}^i(\tau) = (T_{\max} - \tau)\big(- g_i'U_iL_iF_i\big)$$

$$\mathcal{U}_{44}^i(\tau) = (T_{\max} - \tau)\big(2F_i'L_i'U_iL_iF_i\big).$$

The derivative $\dot{V}$ in (18) satisfies

$$\dot{V} = e'(\mathrm{He}(P(A_i + L_iC_i)))e + 2e'(PL_iF_i)f_s + 2e'(P\Delta A_i)e$$

$$+ 2e'P\Delta A_i\hat{\xi} + 2e'(P\Delta A_i)x_e + \hat{\xi}'(\mathrm{He}(PA_i))\hat{\xi}$$

$$- 2\hat{\xi}'(PL_iC_i)e - 2\hat{\xi}'(PL_iF_i)f_s + 2\hat{\xi}'(Pg_i).$$

By applying Lemma 1 in $2e'(P\Delta A_i)e$, $2e'(P\Delta A_i)\hat{\xi}$, and $2e'(P\Delta A_i)x_e$, the following inequality is satisfied

$$0 \geq -\tilde{\zeta}'\mathcal{Q}_i\tilde{\zeta} - \gamma_i\|f_s\|^2 + V + \eta V \tag{24}$$

with $\mathcal{Q}_i, i \in \mathbb{M}$ defined as

$$\mathcal{Q}_i = \begin{bmatrix} \mathcal{Q}_{11}^i & -C_i'L_i'P & 0 & PL_iF_i & 0 & 0 \\ \star & \mathcal{Q}_{22}^i & Pg_i & -PL_iF_i & 0 & 0 \\ \star & \star & \mathcal{Q}_{33}^i & 0 & 0 & 0 \\ \star & \star & \star & -\gamma_{ci}I & 0 & 0 \\ \star & \star & \star & \star & 0 & 0 \\ \star & \star & \star & \star & \star & 0 \end{bmatrix},$$

where $\mathcal{Q}_{11}^i = \mathrm{He}(P(A_i + L_iC_i)) + \eta P + \tilde{\varepsilon}_iN_i'N_i + 3\tilde{\varepsilon}_i^{-1}PM_iM_i'P$, $\mathcal{Q}_{22}^i = \mathrm{He}(PA_i) + \eta P + \tilde{\varepsilon}_iN_i'N_i$, and $\mathcal{Q}_{33}^i = \tilde{\varepsilon}_ix_e'N_i'N_ix_e$.

Considering switching law (9), we obtain $\sigma = i, \forall t \in [t_k, t_{k+1})$ whenever

$$2\hat{\xi}_k' P(A_j\hat{\xi}_k + g_j) - 2\hat{\xi}_k' P(A_i\hat{\xi}_k + g_i) \geq 0, \quad \forall j \in \mathbb{M}. \quad (25)$$

Multiplying (25) by κ_j and summing (25) for all $j \in \mathbb{M}$, after algebraic manipulation we obtain

$$0 \leq 2\hat{\xi}_k'\big(\psi_i(\kappa)\hat{\xi}_k + P(g(\kappa) - g_i)\big) = \tilde{\zeta}' \Xi_i(\tau, \tau^2)\tilde{\zeta}, \quad (26)$$

where $\psi_i = \text{He}(P(A(\kappa) - A_i))$ and

$$\Xi_i(\tau, \tau^2) = \begin{bmatrix} 0 & 0 & 0 & 0 & 0 & 0 \\ \star & \psi_i(\kappa) & -Pg_i & 0 & \tau\psi_i(\kappa) & 0 \\ \star & \star & 0 & 0 & \tau g_i'P & 0 \\ \star & \star & \star & 0 & 0 & 0 \\ \star & \star & \star & \star & \tau^2\psi_i(\kappa) & 0 \\ \star & \star & \star & \star & \star & 0 \end{bmatrix}$$

Summing the right-hand sides of (23) and (26), in (24) using the S-procedure we obtain

$$0 \geq -\tilde{\zeta}' \Xi_i(\tau, \tau^2)\tilde{\zeta} - \gamma_i\|f_s\|^2 - \vartheta_i T_{\max} \\ + \dot{V} + \dot{w} + \eta(V + w)$$

which is equivalent to

$$\dot{\tilde{V}} \leq \tilde{\zeta}' \mathcal{N}_i(\tau, \tau^2)\tilde{\zeta} - \eta\tilde{V} + \gamma_i\|f_s\|^2 + \vartheta_i T_{\max} \quad (27)$$

where $\mathcal{N}_i(\tau, \tau^2) = \mathcal{Q}_i + \mathcal{U}_i(\tau) + \Xi_i(\tau, \tau^2) + (T_{\max} - \tau) (\varepsilon_i^{-1}\tilde{M}_i'\tilde{M}_i + \varepsilon_i\tilde{N}_i'\tilde{N}_i)$. Observe that $\mathcal{N}_i(\tau, \tau^2) \in co\{\mathcal{N}_i(0, 0),$

$\mathcal{N}_i(0, T_{\max}), \mathcal{N}_i(T_{\max}, T_{\max}^2)\}, \forall \tau \in [0, T_{\max}]$, and we obtain $\tilde{\zeta}\mathcal{N}_i(\tau, \tau^2)\tilde{\zeta} < 0$ if

$$\tilde{\zeta}' \mathcal{N}_i(0, 0)\tilde{\zeta} \leq 0 \quad (28)$$
$$\tilde{\zeta}' \mathcal{N}_i(0, T_{\max})\tilde{\zeta} \leq 0 \quad (29)$$
$$\tilde{\zeta}' \mathcal{N}_i(T_{\max}, T_{\max}^2)\tilde{\zeta} \leq 0. \quad (30)$$

When $\tau = 0$, we have $t = t_k$ and $\hat{\xi}(t) = \hat{\xi}_k$, $e(t) = e_k$, thus $\hat{\varphi}(t) = \varphi(t) = 0$, and inequality (28) is satisfied whenever

$$\overline{\zeta}' \tilde{\mathcal{N}}_i(0, 0)\overline{\zeta} \leq 0 \quad (31)$$

where $\overline{\zeta} := \begin{bmatrix} e' & \hat{\xi}' & 1 & f_s' \end{bmatrix}'$ and $\tilde{\mathcal{N}}_i(0, 0)$ with compatible dimensions is obtained by removing the last columns and rows of $\mathcal{N}_i(0, 0)$. Applying Schur's complement in $\tilde{\mathcal{N}}_i(0, 0)$ and $\mathcal{N}_i(T_{\max}, T_{\max}^2)$ we obtain (15) and (16), respectively, If there exist matrices P, U_i, L_i and parameters $\tilde{\varepsilon}_i, \varepsilon_i, \vartheta_i, \gamma_i$ that satisfies the problem of minimizing α subject to inequalities (12), (13) and (14) than the inequalities (28)-(30) hold[2] and the derivative in (27) satisfies

$$\dot{\tilde{V}} \leq -\eta\tilde{V} + \gamma_i\|f_s\|^2 + \vartheta_i T_{\max}. \quad (32)$$
$$\leq -\eta\tilde{V} + \gamma_i\beta_f^2 + \vartheta_i T_{\max} \quad (33)$$
$$< -\eta\tilde{V} + \alpha\eta T_{\max} \quad (34)$$

[2]Note that (30) implies (29) and (28) is satisfied when (31) holds.

$$\mathcal{M}_i(0, 0) = \begin{bmatrix} \mathcal{M}_{11}^i(0) & \mathcal{M}_{12}^i(0) & \mathcal{M}_{13}^i(0) & PL_iF_i + T_{\max}\big((2C_i'L_i' + A_i'U_i)L_iF_i\big) & PM_i & (A_i + L_iC_i)'U_iM_i \\ \star & \mathcal{M}_{22}^i(0) & \mathcal{M}_{23}^i(0) & -PL_iF_i - T_{\max}(A_i'U_iL_iF_i) & 0 & 0 \\ \star & \star & \mathcal{M}_{33}^i(0) & -T_{\max}\big(g_i'U_iL_iF_i\big) & 0 & 0 \\ \star & \star & \star & -\gamma_iI + T_{\max}\big(2F_i'L_iU_iL_iF_i\big) & 0 & F_i'L_i'U_iM_i \\ \star & \star & \star & \star & -3\tilde{\varepsilon}_iI & 0 \\ \star & \star & \star & \star & \star & -\varepsilon_i(T_{\max})^{-1}I \end{bmatrix}$$

$$(15)$$

$$\mathcal{M}_i(T_{\max}, T_{\max}^2) = \begin{bmatrix} \mathcal{M}_{11}^i(T_{\max}) & -C_i'L_i'P & 0 & PL_iF_i & 0 & 0 & PM_i \\ \star & \mathcal{M}_{22}^i(T_{\max}) & 0 & -PL_iF_i & -T_{\max}\psi_i(\kappa) & 0 & 0 \\ \star & \star & \mathcal{M}_{33}^i(T_{\max}) & 0 & T_{\max}g_i'P & 0 & 0 \\ \star & \star & \star & -\gamma_iI & 0 & 0 & 0 \\ \star & \star & \star & \star & \mathcal{M}_{55}^i(T_{\max}, T_{\max}^2) & 0 & 0 \\ \star & \star & \star & \star & \star & \mathcal{M}_{66}^i(T_{\max}) & 0 \\ \star & \star & \star & \star & \star & \star & -3\tilde{\varepsilon}_iI \end{bmatrix}$$

$$(16)$$

with $\mathcal{M}_{55}^i(\tau, \tau^2) = -\tau U_ie^{-\eta T_{\max}} + \tau^2\psi_i(\kappa)$, $\mathcal{M}_{66}^i(\tau) = -\tau U_ie^{-\eta T_{\max}}$ and

$$\mathcal{M}_{11}^i(\tau) = \text{He}(P(A_i + L_iC_i)) + \eta P + \tilde{\varepsilon}_iN_i'N_i + \psi_i(\kappa) + (T_{\max} - \tau)\big((A_i' + C_i'L_i')U_iA_i + A_i'U_iL_iC_i + 2C_i'L_i'U_iL_iC_i \\ + Q_i'U_iQ_i + \varepsilon_iN_i'N_i\big),$$

$$\mathcal{M}_{12}^i(\tau) = -C_i'L_i'P + (T_{\max} - \tau)\big(-C_i'L_i'U_iA_i + Q_i'U_iQ_i + \varepsilon_iN_i'N_i\big),$$

$$\mathcal{M}_{13}^i(\tau) = (T_{\max} - \tau)\big(-C_i'L_i'U_ig_i + Q_i'U_iQ_ix_e + \varepsilon_iN_i'N_ix_e\big),$$

$$\mathcal{M}_{22}^i(\tau) = \text{He}(PA_i) + \eta P + \tilde{\varepsilon}_iN_i'N_i + \psi_i(\kappa) + (T_{\max} - \tau)\big(A_i'U_iA_i + Q_i'U_iQ_i + \varepsilon_iN_i'N_i\big),$$

$$\mathcal{M}_{23}^i(\tau) = (T_{\max} - \tau)\big(A_i'U_ig_i + Q_i'U_iQ_ix_e + \varepsilon_iN_i'N_ix_e\big),$$

$$\mathcal{M}_{33}^i(\tau) = -\vartheta_i T_{\max} + x_e'\tilde{\varepsilon}_iN_i'N_ix_e + (T_{\max} - \tau)\big(g_i'U_ig_i + x_e'Q_i'U_iQ_ix_e + \varepsilon_ix_e'N_i'N_ix_e\big)$$

where (32) is obtained by considering inequality (3), and inequality (34) is obtained using (14). From (34), inequality (20) holds, and by the comparison principle, from (34) we obtain

$$\tilde{V}(\zeta(t)) < e^{-\eta t}\tilde{V}(0) + \alpha T_{\max} \int_0^t e^{-\eta(t-s)}\eta ds \quad (35)$$

$$= e^{-\eta(t)}(\tilde{V}(0) - \alpha T_{\max}) + \alpha T_{\max}. \quad (36)$$

When (20) is satisfied, then $\dot{\tilde{V}} = \dot{V}(t) + \dot{w}(t) < 0$ whenever $V(t) \geq \alpha T_{\max} - w(t)$, where the latter inequalities hold for any $\zeta \notin \Omega$, since $w(t) \geq 0, \forall t \geq 0$, implying that Ω is an attractor set for augmented system (7). Now we prove by contradiction that if $\zeta(t_k) \in \Omega$ for some $k \in \mathbb{N}$, then $\zeta(t) \in \Omega, \forall t \geq t_k$. Let $\zeta(t_k) \in \Omega$ and assume that for some $t_l \in (t_k, t_{k+1})$ we have $V(\zeta(t_l)) = \alpha T_{\max} - w(t_l)$ and that $V(\zeta(s)) \geq \alpha T_{\max} - w(s), \forall s \in (t_l, t] \subset (t_k, t_{k+1})$. Then $\dot{V}(\zeta(s)) + \dot{w}(s) < 0$ for all $s \in (t_l, t]$, which after integration leads to $V(\zeta(t)) + w(t) < V(\zeta(t_l)) + w(t_l) = \alpha T_{\max}$. We then obtain $V(\zeta(t)) < \alpha T_{\max} - w(t), \forall t \in [t_k, t_{k+1})$ which is a contradiction. Therefore, the trajectories of (7) are attracted to (10) as $t \to \infty$, and the solution cannot exit Ω between sampling instants. Moreover, ζ in (7) satisfies $\|\zeta\|^2 = \|e\|^2 + \|\hat{\xi}\|^2 = \|x - \hat{x}\|^2 + \|\hat{x} - x_e\|^2$. Therefore, $\|x - x_e\|^2 \leq (\|e\| + \|\hat{\xi}\|)^2 \leq 2(\|e\|^2 + \|\hat{\xi}\|^2) = 2\|\zeta\|^2$. Hence, from (10), we obtain the ball in (8) where $\omega = \sqrt{2\alpha T_{\max}/\lambda_{\min}(P)}$ is the minimum radius for a given P obtained by minimizing α. $\square$

Remark 2: The Lyapunov-Krasowskii functional (17) in Theorem 1 was considered instead of the classical Lyapunov function since switching law (9) is sampled-based, which makes the switching between system modes be time-delayed by $\tau(t) = t - t_k$. Therefore, the solution of the switched system in (7) obtained by applying a sampled-data-based switching is also time-delayed. For more details of this approach, see [27].

Theorem 1 yields the conditions to verify if the observer-based strategy makes the trajectories of (7) be attracted to the ball $\mathcal{B}(x_e, \omega)$, defined in (8), with the smallest radius ω. However, conditions (12)-(14) are not LMIs and have complex numerical solutions. Thus, in the next theorem, we propose LMI-based conditions to obtain an approximate solution of the optimization problem in Theorem 1 at the cost of increasing the ball for which the trajectories of system (7) are attracted to the ball which is defined by

$$\mathcal{B}(x_e, \overline{\omega}) := \left\{ x \in \mathbb{R}^n : \|x - x_e\|^2 < \overline{\omega}^2 \right\}, \quad (37)$$

for a given $\kappa \in \mathbb{K}$, $x_e \in \mathcal{X}_e$ and all $\|f_s\| \leq \beta_f$. The value of $\overline{\omega}$ is given in terms of LMIs.

Theorem 2: Given $\kappa \in \mathbb{K}$, $x_e \in \mathcal{X}_e$ satisfying (4), $\overline{\alpha}_i > 0$, $\forall i \in \mathbb{M}$, $\eta > 0$ and a maximum sample $T_{\max} > 0$, if there exist positive definite matrices $P \in \mathbb{R}^{n \times n}$, $U_i \in \mathbb{R}^{n \times n}$, negative definite matrices $V_i \in \mathbb{R}^{n \times n}$, general matrices $L_i \in \mathbb{R}^{n \times p}$ and positive parameters $\tilde{\varepsilon}_i, \varepsilon_i, \vartheta_i, \gamma_i$ solution of the optimization problem (38)-(41), for all $(\sigma(t_k) = i, \sigma(t_k^-) = j) \in \mathbb{M} \times \mathbb{M}, i \neq j$, then, practical stability of system (7) is guaranteed and the trajectories are attracted to ball (37),

with $\overline{\omega} = \sqrt{2\overline{\alpha}T_{\max}/\lambda_{\min}(P)}$ and $\overline{\alpha} = \max_{i \in \mathbb{M}}(\overline{\alpha}_i)$, when $t \to \infty$. Moreover, the observer gains are obtained as $L_i = (V_i')^{-1}Y_i, \forall i \in \mathbb{M}$.

$$\min_{P, U_i, \gamma_i, \tilde{\varepsilon}_i, \varepsilon_i, \vartheta_i} - \ln(\det(P)), \quad (38)$$

$$\text{subject to: } \Psi_i(0, 0) + \text{He}((\mathcal{G}_0^i)'V_i\mathcal{H}_0^i) \preceq 0 \quad (39)$$

$$\Psi_i(T_{\max}, T_{\max}^2) + \text{He}((\mathcal{G}_{T_{\max}}^i)'V_i\mathcal{H}_{T_{\max}}^i) \preceq 0, \quad (40)$$

$$\overline{\alpha}_i\eta T_{\max} - \vartheta_i T_{\max} - \gamma_i\beta_f^2 > 0 \quad (41)$$

where matrices $\Psi_i(0, 0)$, $\Psi_i(T_{\max}, T_{\max}^2)$ are defined in (48) and (49), as shown at the bottom of the next page, respectively, with $Y_i = V_i'L_i$ and

$$\mathcal{G}_0^i = [I \ L_iC_i \ -L_iC_i \ 0.5g_i \ -L_iF_i \ 0 \ 0]$$
$$\mathcal{G}_{T_{\max}}^i = [I \ L_iC_i \ -L_iC_i \ 0 \ -L_iF_i \ 0 \ 0 \ 0]$$
$$\mathcal{H}_0^i = [I \ 0 \ 0 \ 0 \ 0 \ 0 \ 0], \quad \mathcal{H}_{T_{\max}}^i = [I \ 0 \ 0 \ 0 \ 0 \ 0 \ 0 \ 0],$$

proof: Considering functional (20), derivative $\dot{\tilde{V}}$ satisfies (32). Applying Schur's complement to $\mathcal{N}_i(\tau, \tau^2)$ and from the convexity properties we obtain the matrices $\mathcal{M}_i(0, 0)$ in (15) and $\mathcal{M}_i(T_{\max}, T_{\max}^2)$ in (16). In addition, inequalities (12) and (13) can be expressed as follows:

$$(N_{\mathcal{G}_0}^i)'\Psi_i(0, 0)N_{\mathcal{G}_0}^i \preceq 0 \quad (42)$$

$$(N_{\mathcal{G}_{T_{\max}}}^i)'\Psi_i(T_{\max}, T_{\max}^2)N_{\mathcal{G}_{T_{\max}}}^i \preceq 0 \quad (43)$$

with

$$N_{\mathcal{G}_0}^i = \begin{bmatrix} L_iC_i & 0 & -0.5g_i & L_iF_i & 0 & 0 \\ I & -I & 0 & 0 & 0 & 0 \\ \hline \mathbf{0}_{(3n+p+1)\times n} & \mathbf{I}_{(3n+p+1)\times(3n+p+1)} \end{bmatrix}$$

$$N_{\mathcal{G}_{T_{\max}}}^i = \begin{bmatrix} L_iC_i & 0 & 0 & L_iF_i & 0 & 0 \\ I & -I & 0 & 0 & 0 & 0 \\ \hline \mathbf{0}_{(4n+p+1)\times n} & \mathbf{I}_{(4n+p+1)\times(4n+p+1)} \end{bmatrix}$$

Also, we have that $-\gamma_iI \prec 0, \forall i \in \mathbb{M}$, since γ_i is assumed to be positive for all $i \in \mathbb{M}$, which corresponds to

$$(N_{\mathcal{H}_0}^i)'\Psi_i(0, 0)N_{\mathcal{H}_0}^i \preceq 0 \quad (44)$$

$$(N_{\mathcal{H}_{T_{\max}}}^i)'\Psi_i(T_{\max}, T_{\max}^2)N_{\mathcal{H}_{T_{\max}}}^i \preceq 0 \quad (45)$$

with

$$N_{\mathcal{H}_0}^i = \begin{bmatrix} \mathbf{0}_{(3n+1)\times(2n+1)} & \mathbf{0}_{(3n+1)\times p} & \mathbf{0}_{(3n+1)\times(2n+1)} \\ \mathbf{0}_{p\times(2n+1)} & \mathbf{I}_{p\times p} & \mathbf{0}_{p\times(2n+1)} \\ \mathbf{0}_{2n\times(2n+1)} & \mathbf{0}_{2n\times p} & \mathbf{0}_{2n\times(2n+1)} \end{bmatrix}$$

$$N_{\mathcal{H}_{T_{\max}}}^i = \begin{bmatrix} \mathbf{0}_{(3n+1)\times(2n+1)} & \mathbf{0}_{(3n+1)\times p} & \mathbf{0}_{(3n+1)\times(3n+1)} \\ \mathbf{0}_{p\times(2n+1)} & \mathbf{I}_{p\times p} & \mathbf{0}_{p\times(3n+1)} \\ \mathbf{0}_{3n\times(2n+1)} & \mathbf{0}_{2n\times p} & \mathbf{0}_{3n\times(3n+1)}. \end{bmatrix}$$

Consider $\mathcal{G}_i(0) \in \text{Null}(N_{\mathcal{G}}^i(0))$, $\mathcal{G}_i(T_{\max}) \in \text{Null}(N_{\mathcal{G}}^i(T_{\max}))$, $\mathcal{H}_i(0) \in \text{Null}(N_{\mathcal{H}}^i(0))$, $\mathcal{G}_i(T_{\max}) \in \text{Null}(N_{\mathcal{H}}^i(T_{\max}))$. From Lemma 2, there exists a matrix V_i that satisfies (39) and (40) if (42)-(45) hold. Thus, by solving (39) and (40) we guarantee that (42)-(45) hold, and consequently,

LMIs (12)-(13) in Theorem 1 are also satisfied. Hence, the following inequalities hold:

$$\dot{\tilde{V}} \le -\eta\tilde{V} + \gamma_i\|f_s\|^2 + \vartheta_i T_{\max}. \quad (46)$$

$$< -\eta\tilde{V} + \overline{\alpha}\eta T_{\max} \quad (47)$$

where (46) is obtained by considering the bound in Assumption 2 and inequality (47) is obtained by solving (41). Note that (47) is the same as (34) in Theorem 1 by taking $\overline{\alpha} = \alpha$. By following the same steps as those in the proof of Theorem 1, we can show that the trajectories of (7) are attracted to (37). In addition, by maximizing $\ln(\det(P))$, the eigenvalues of P^{-1} are minimized, which minimizes $\overline{\omega}$. $\square$

A. ESTIMATION OF THE REGION OF ATTRACTION

The radius $\overline{\omega}$ of (37) obtained by Theorem 2 is a conservative estimation of the region of attraction $\mathcal{B}(x_e, \omega)$ from (8), since the values of $\overline{\alpha}_i$ are given. A simple way to improve the estimation of the region $\mathcal{B}(x_e, \omega)$ is to use the solution of Theorem 2 (matrices P and L_i) to convert (12) and (13), from Theorem 1, into LMIs. The next theorem formalizes this strategy.

Theorem 3: For given $\kappa \in \mathbb{K}$, $x_e \in \mathcal{X}_e$ satisfying (4), $\eta > 0$, $\overline{\alpha}_i > 0$, $\forall i \in \mathbb{M}$, a maximum sample time $T_{\max} > 0$, and P, L_i solutions of Theorem 2, if there exist positive definite matrices $U_i \in \mathbb{R}^{n \times n}$ and positive parameters $\tilde{\varepsilon}_i$, ε_i, ϑ_i, γ_i, α, satisfying the optimization problem (11)-(14), for all $(\sigma(t_k) = i, \sigma(t_k^-) = j) \in \mathbb{M} \times \mathbb{M}$, $i \ne j$, then, the practical stability of system (7) is guaranteed and the trajectories are attracted to (10), for the switching law given in (9), with $\mathcal{P} := \text{diag}([P, P])$. Furthermore, the trajectories

of (1) are attracted to (8) with a minimum radius denoted by ω.

Proof: The proof is immediate, considering matrices P and L_i as known, and following the same steps as those in the proof of Theorem 1. $\square$

Remark 3: The region $\mathcal{B}(x_e, \overline{\omega})$ obtained using Theorem 2 can be reduced in Theorem 3 by minimizing α for the given matrices P and L_i. In this case, we obtain region (8), such that $\omega \le \overline{\omega}$, and $\alpha \le \overline{\alpha}$. Moreover, from Lemma 2, inequalities (12) and (13) are satisfied whenever all the conditions in Theorem 2 hold, which means that in the worst case of the solution of Theorem 3, we obtain $\alpha = \overline{\alpha}$, and $\omega = \overline{\omega}$.

B. OBTAINING THE OBSERVER AND SWITCHING LAW MATRICES SYSTEMATICALLY

For the feasibility of (39) and (40) in Theorem 2, the real part of the eigenvalues of $(A(\kappa) + (\eta/2)I)$ must be negative, implying that $A(\kappa)$ must be Hurwitz. Furthermore, inequalities (39) and (40) hold if the real part of the eigenvalues of $(A(\kappa) + \Delta A_i + (\eta/2)I)$ is negative for all $\tilde{\delta}_i \in [-1, 1]$, $i \in \mathbb{M}$. Thus η must satisfy

$$0 < \eta < -2\overline{\lambda}_{\max}(A(\kappa) + \delta_{ai}Q_i), \quad \forall\delta_{ai} \in [-1, 1], \ i \in \mathbb{M}. \quad (50)$$

In addition, by applying switching law (9) in the augmented system in (7) it is not necessary to guarantee that the pairs (A_i, C_i) are observable for all $i \in \mathbb{M}$ to solve the optimization problems (11)-(14) and (38)-(41), for all $(\sigma(t_k) = i, \sigma(t_k^-) = j) \in \mathbb{M} \times \mathbb{M}$, $i \ne j$. On the other hand, we need to

$$\Psi_i(0,0) = \begin{bmatrix} 2T_{\max}U_i & (P+T_{\max}U_iA_i) & 0 & 0 & 0 & 0 & U_iM_i \\ \star & \Psi_{22}^i(0) & \Psi_{23}^i(0) & \Psi_{24}^i(0) & 0 & PM_i & A_i'U_iM_i \\ \star & \star & \Psi_{33}^i(0) & T_{\max}(A_i'U_ig_i) & 0 & -PM_i & -A_i'U_iM_i \\ \star & \star & \star & \Psi_{44}^i(0) & 0 & 0 & 0.5g_i'U_iM_i \\ \star & \star & \star & \star & -\gamma_iI & 0 & 0 \\ \star & \star & \star & \star & \star & -3\tilde{\varepsilon}_iI & 0 \\ \star & \star & \star & \star & \star & \star & -T_{\max}^{-1}\varepsilon_iI \end{bmatrix} \quad (48)$$

$$\Psi_i(T_{\max}, T_{\max}^2) = \begin{bmatrix} 0 & P & 0 & 0 & 0 & 0 & 0 & 0 \\ \star & \Psi_{22}^i(T_{\max}) & \Psi_{23}^i(T_{\max}) & 0 & 0 & 0 & 0 & PM_i \\ \star & \star & \Psi_{33}^i(T_{\max}) & 0 & 0 & -T_{\max}\psi_i(\kappa) & 0 & -PM_i \\ \star & \star & \star & \Psi_{44}^i(T_{\max}) & 0 & T_{\max}g_i'P & 0 & 0 \\ \star & \star & \star & \star & -\gamma_iI & 0 & 0 & 0 \\ \star & \star & \star & \star & \star & \Psi_{66}^i(T_{\max}) & 0 & 0 \\ \star & \star & \star & \star & \star & \star & -T_{\max}U_ie^{-\eta T_{\max}} & 0 \\ \star & \star & \star & \star & \star & \star & \star & -3\tilde{\varepsilon}_iI \end{bmatrix} \quad (49)$$

with $\Psi_{33}^i(\tau) = \Psi_{23}^i(\tau) + \Psi_{23}^i(\tau)'$, $\Psi_{55}^i(\tau, \tau^2) = -\tau U_ie^{-\eta T_{\max}} + \tau^2\psi_i(\kappa)$ and

$$\Psi_{22}^i(\tau) = \text{He}(PA_i) + \psi_i(\kappa) + \eta P + \tilde{\varepsilon}_iN_i'N_i + (T_{\max} - \tau)(A_i'U_iA_i + Q_i'U_iQ_i + \varepsilon_iN_i'N_i)$$

$$\Psi_{23}^i(\tau) = \Psi_{22}^i(\tau) + (T_{\max} - \tau)(Q_i'U_iQ_i + \varepsilon_iN_i'N_i)$$

$$\Psi_{24}^i(\tau) = 0.5(P + T_{\max}A_i'U_i)g_i + T_{\max}(Q_iU_iQ_ix_e + \varepsilon_iN_i'N_ix_e)$$

$$\Psi_{44}^i(\tau) = -\vartheta_iT_{\max} + \tilde{\varepsilon}_ix_e'N_i'N_ix_e + (T_{\max} - \tau)(x_e'Q_i'U_iQ_ix_e + \varepsilon_ix_e'N_i'N_ix_e + 0.5g_i'U_ig_i)$$

guarantee that the eigenvalues of the matrices in the diagonals of $\mathcal{M}_i(0,0)$ in (12) and $\mathcal{M}_i(T_{\max}, T_{\max}^2)$ in (13) are negative to satisfy (12) and (13). Moreover, (39) and (40) are satisfied only if there exist matrices and parameters that satisfy (12) and (13). Thus, to find a solution to (12), (13), (39) and (49), it is necessary to ensure that there exists κ, P and L_i satisfying

$$\text{He}(P(A(\kappa) + L_i C_i)) \prec 0 \quad \forall i \in \mathbb{M}, \qquad (51)$$

and η satisfying (50). Therefore, the pairs $(A(\kappa), C_i)$ must be observable for all $i \in \mathbb{M}$. Furthermore, to obtain the gain matrices L_i and switching law matrix P, consider the following algorithm.

Algorithm 1 Obtaining the Observer and Switching Law Matrices

---
Require: $\kappa \in \mathbb{K}$ such that the pairs $(A(\kappa), C_i)$ are observable for all $i \in \mathbb{M}$
Require: η satisfying (50),
Require: $T_{\max} = 1/f_{sw}$ where f_{sw} is the minimum switching frequency as in Remark 1.
Require: $\overline{\alpha}_i > 0, \forall i \in \mathbb{M}$
  if A solver for nonlinear matrix inequalities is available **then**
    Solve the optimization problem (11)-(14), for all $(\sigma(t_k) = i, \ \sigma(t_k^-) = j) \in \mathbb{M} \times \mathbb{M}, i \neq j$ in Theorem 1.

    Return observer and switching law matrices L_i and P for all $i \in \mathbb{M}$.
    Return radius ω, with $\omega = \sqrt{2\alpha T_{\max}/\lambda_{\min}(P)}$
  else
    Solve the optimization problem (38)-(41) for all $(\sigma(t_k) = i, \ \sigma(t_k^-) = j) \in \mathbb{M} \times \mathbb{M}, i \neq j$ in Theorem 2.

    Return observer and switching law matrices L_i and P for all $i \in \mathbb{M}$.
    Return radius $\overline{\omega}$ with $\overline{\omega} = \sqrt{2\overline{\alpha} T_{\max}/\lambda_{\min}(P)}$ and $\overline{\alpha} = \max_{i \in \mathbb{M}}(\overline{\alpha}_i)$
    With L_i and P, solve the optimization problem (11)-(14), for all $(\sigma(t_k) = i, \ \sigma(t_k^-) = j) \in \mathbb{M} \times \mathbb{M}, i \neq j$ as in Theorem 3
    Return radius ω, with $\omega = \sqrt{2\alpha T_{\max}/\lambda_{\min}(P)}$
  end if

The matrices obtained by solving the optimization problems in Theorem 1 or 2 guarantee that the trajectory of system (1) is attracted to (8) for a fixed equilibrium point $x_e \in \mathcal{X}_e$ when switching law (9) is considered. Moreover, if is not possible to solve the optimization problem in Theorem 1, then the estimation of the region of attraction is obtained using Theorem 3. Otherwise, Theorem 1 provides the gains and the estimation of the the region of attraction. In the next section, we propose an algorithm to determine a set of equilibrium points where x is attracted to (8) with the same radius ω obtained in Theorem 3, considering the same gain

matrix P and observer matrices L_i for a special case in which the number of system modes $M = 2$.

C. SEARCH FOR EQUILIBRIUM POINTS
Define a set of equilibrium points Ω_{x_e} as

$$\Omega_{x_e} = \{x_e \in \mathcal{X}_e : x_e \in \mathcal{B}(x_e, \omega)\} \qquad (52)$$

which means that $\Omega_{x_e} \subseteq \mathcal{X}_e$. For two modes, any equilibrium point $x_e \in \mathcal{X}_e$ can be obtained by a proper choice of $\overline{\kappa}$ that satisfies $0 < \overline{\kappa} < 1$, such that $x_e = -((\overline{\kappa}A_1 + (1-\overline{\kappa})A_2)^{-1}(\overline{\kappa}b_1 + (1-\overline{\kappa})b_2)$. Consider now $\overline{\Omega}_{x_e} \subseteq \Omega_{x_e}$. By applying Algorithm 2, we obtain $\overline{\Omega}_{x_e}$ for known matrices P and L_i, where $\kappa_{\text{steps}} \in \mathbb{R}, 0 < \kappa_{\text{steps}} < 1$ is the increment in $\overline{\kappa}$.

Algorithm 2 Search for the Equilibrium Points

Require: Matrices P, L_i and a number $\alpha > 0$ obtained in Theorem 3.
  $\overline{\kappa} \leftarrow \kappa_{\text{steps}}$
  $\overline{\Omega}_{x_e}$ is empty
  while $\overline{\kappa} < 1$ **do**
    $x_e \leftarrow -((\overline{\kappa}A_1 + (1-\overline{\kappa})A_2)^{-1}(\overline{\kappa}b_1 + (1-\overline{\kappa})b_2)$
    if (12)-(14) are satisfied, $\forall \sigma = i, i \in \mathbb{M}$, **then**
      $\overline{\Omega}_{x_e} \leftarrow \overline{\Omega}_{x_e} \cup x_e$
    end if
    $\overline{\kappa} \leftarrow \overline{\kappa} + \kappa_{\text{steps}}$
  end while

Remark 4: For observer matrices L_i, $i \in \mathbb{M}$ and switching law gain in (9) given by Theorem 2, a given radius ω is obtained in Theorem 3 and for any equilibrium point in $\overline{\Omega}_{x_e}$, Algorithm 2 provides a condition to guarantee that, the trajectories of (7) are attracted to $\mathcal{B}(x_e, \omega)$, for any initial condition. However, if an equilibrium point $x_c \in \mathcal{X}_e$ does not belong to $\overline{\Omega}_{x_e}$, it does not necessarily mean that system (7) is unstable when applying the switching law (9) with the matrix P and the observer gains L_i, instead, x_c may belong to a set where the radius of the ball is greater than the optimum radius ω obtained in Theorem 3. Moreover, using Algorithm 2, we cannot obtain all the elements of set (52), but it is possible to obtain a greater number of elements for small values of κ_{steps}.

V. EXPERIMENTAL RESULTS
To illustrate the fault-tolerant switching law strategy proposed in this paper, we considered a bidirectional buck-boost DC–DC converter with a battery as the input voltage source. The converter is shown in Figure 2, where i_L is the inductor current, v_C is the output capacitor voltage, L_{in} is the inductance with a loss r_L, r_S is the switching device loss, C_v is the capacitance, R_o is the load resistance and v_{bat} is the input voltage source with an internal resistance r_{bat}. The converter, subject to persistent bounded sensor faults, was modeled as system (1) with $x = [i_L \ v_C]'$ for $\sigma = i, \forall i \in \{1, 2\}$,
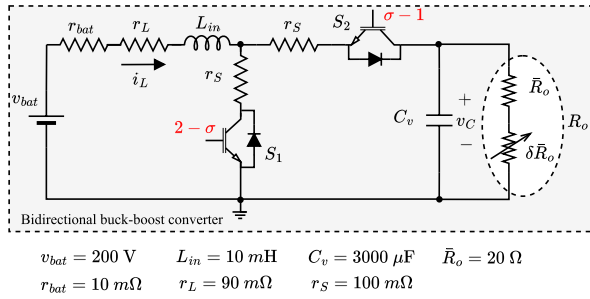
$$v_{bat} = 200 \text{ V} \quad L_{in} = 10 \text{ mH} \quad C_v = 3000 \text{ }\mu\text{F} \quad \overline{R}_o = 20 \text{ }\Omega$$
$$r_{bat} = 10 \text{ m}\Omega \quad r_L = 90 \text{ m}\Omega \quad r_S = 100 \text{ m}\Omega$$

FIGURE 2. Bidirectional buck-boost DC–DC converter. The subtraction in the switching signal corresponds to the modes 1 and 0, representing the 'on' and 'off' states of the switching device, respectively. Note that when the switching device S_1 is active, the switching S_2 is inactive.

$B_1 = B_2 = [1/L_{in} \ 0]'$, $u = v_{bat}$, $b_1 = b_2 = B_1u = [v_{bat}/L_{in} \ 0]'$, $C_1 = C_2 = [0 \ 1]$, $F_1 = F_2 = 1$ and:

$$A_{\sigma=1} = \begin{bmatrix} -\dfrac{r_{eq}}{L_{in}} & 0 \\ 0 & -\dfrac{1}{\overline{R}_oC_v} \end{bmatrix}, \quad A_{\sigma=2} = \begin{bmatrix} -\dfrac{r_{eq}}{L_{in}} & -\dfrac{1}{L_{in}} \\ \dfrac{1}{C_v} & \dfrac{-1}{\overline{R}_oC_v} \end{bmatrix}$$

where $r_{eq} = r_{bat} + r_L + r_S$ and indices 1 and 2 correspond to the on and off state of switching devices S_1 and S_2, respectively, activated in a complementary manner.

Considering a variation of 50% in the load resistance, the uncertainties ΔA_1 and ΔA_2 are described according to (2) as follows:

$$Q_1 = Q_2 = \begin{bmatrix} 0 & 0 \\ 0 & \dfrac{\delta R_o}{(1+\delta R_o)R_oC_v} \end{bmatrix}, \quad \delta = 0.5$$

$$M_1 = M_2 = \begin{bmatrix} 0 & 0 \\ \dfrac{\delta R_o}{(1+\delta R_o)R_oC_v} & 0 \end{bmatrix}, \quad N_1 = N_2 = \begin{bmatrix} 0 & 1 \\ 0 & 0 \end{bmatrix}.$$

Next, considering that switching law (9) is applied to the proposed bidirectional buck-boost converter, we present the design of the observer gain in (7) and matrix P in (9), along with the experimental results for different scenarios, considering changes in equilibrium points, load variations and sensor faults.

A. DESIGN OF THE OBSERVER GAINS AND SWITCHING LAW

First, denoting i_{Le} and v_{Ce} as the inductor current and voltage sensor in equilibrium, respectively, an equilibrium point $x_e \in \mathcal{X}_e$ is chosen to be $x_e = [i_{Le} \ v_{Ce}]' = [38.462 \ 384.615]'$, for $\kappa = [0.50 \ 0.50]$, where $i_{Le} = 38.462$ A and $v_{Ce} = 348.615$ V

Moreover, we considered persistent bounded sensor faults with a maximum magnitude of $\beta_f = 192.308$ V, representing a maximum offset of $0.5v_{Ce}$, which means that we aim to design observer gains to guarantee a fault tolerance of the converter against any absolute value for fault magnitude below or equal to β_f under the sampled-observer based switching law (9). Additionally, practical stability of (7) is guaranteed when a switching frequency of at least 10 kHz

is applied.[3] Hence, we defined a fixed sample time $T_k = T_{max} = 10^{-4}$ s, $\forall k \in \mathbb{N}$ for system (1).

Once we have established all the requirements for the switching law design, the observer gains and switching law can be obtained by solving the optimization problem in Theorem 2, whereas the radius of (8) can be obtained by solving the optimization problem in Theorem 3, considering matrices A_i, b_i, C_i, F_i, M_i, N_i and Q_i for all $i \in \mathbb{M}$ obtained for the uncertain DC–DC converter.

However, to cope with large numerical values in the system matrices and to avoid ill-conditioned matrix inequalities, we considered a time scale change in system (7), such that the system of the form (7) is obtained with $\tilde{A}_i = \epsilon^{-1}\overline{A}_i$, $\tilde{M}_i = \epsilon^{-1}\overline{F}_i$, $\tilde{C}_i = \epsilon^{-1}\overline{C}_i$ and $\tilde{T}_{max} = \epsilon T_{max}$, where $\epsilon = 10^4$ is the time scaling constant, as considered in [27]. Observe that the switching law obtained considering the time scale change is equivalent to switching law[4] (9), since $\sigma(\hat{\xi}_k) = \arg\min_{i\in\mathbb{M}}(\hat{\xi}'_k P(A_i\hat{\xi}_k + g_i)) = \arg\min_{i\in\mathbb{M}}(\hat{\xi}'_k P(\epsilon A_i\hat{\xi}_k + \epsilon g_i))$, $\forall i \in \mathbb{M}$. Then, by solving the optimization problem proposed in Theorem 2, with $\eta = 16.67 \times 10^{-4}$ satisfying (50), $\alpha_1 = \alpha_2 = 10^4$, and $\beta_f = 192.308$ V, we obtain the following matrices:

$$P = \begin{bmatrix} 0.0212 & -0.0001 \\ -0.0001 & 0.0067 \end{bmatrix}, \quad L_1 = \begin{bmatrix} 0.0033 \\ -0.0011 \end{bmatrix},$$
$$L_2 = 10^{-3} \times \begin{bmatrix} -0.06157 \\ 0.2022 \end{bmatrix},$$

and the radius of (37) is obtained as $\overline{\omega} = 1.723 \times 10^3$. It can be verified that $\overline{\omega}$ represents a very high value for the radius of the ball where the trajectories of (1) converge under uncertainties and sensor faults. Nonetheless, by applying P and L_i in Theorem 3, for all $i \in \mathbb{M}$, we obtain the minimum radius of (8), which corresponds to $\omega = 184.796$. In general, most of the parameters obtained as a solution for the optimization problem proposed in Theorem 3 yield smaller attraction region than the obtained in Theorem 2, since $\overline{\alpha}_i < \alpha$, $\forall i \in \mathbb{M}$, as we can see in Table 1.

TABLE 1. Parameters obtained applying theorems 2 and 3.

Theorem	i	$\tilde{\varepsilon}_i$	ε_i	γ_i	ϑ_i
2	1	0.0433	7.639×10^{-5}	1.708×10^{-7}	16.662
	2	0.0446	1.765×10^{-5}	1.002×10^{-8}	16.67
3	1	0.0058	5.845×10^{-4}	1.746×10^{-7}	0.182
	2	0.0066	$3.986.1 \times 10^{-5}$	1×10^{-9}	0.191

In addition, by applying Algorithm 2 with $\kappa_{steps} = 0.050$, we obtained the set of all equilibrium points that satisfy (52), the elements of which are listed in Tables 2 and 3, where each column composed of i_{Le} and v_{Ce} for a given κ is an element of $\overline{\Omega}_{x_e}$.

---

[3]This value corresponds to a common operational frequency for power electronic switching devices, as mentioned in the introduction.

[4]The value of the minimum obtained after the time scaling is not the same. However, since ϵ multiplies $\hat{\xi}'_k P(A_i\hat{\xi}_k + g_i)$ for all $i \in \mathbb{M}$, then the argument i remains the same.

TABLE 2. Equilibrium points for $0.05 \leq \overline{\kappa} \leq 0.25$.

State variable	$\overline{\kappa}$				
	0.05	0.10	0.15	0.20	0.25
i_{Le}	10.959	12.195	13.6519	15.385	17.467
v_{Ce}	208.219	219.512	232.082	246.154	262.009

TABLE 3. Equilibrium points for $0.30 \leq \overline{\kappa} \leq 0.50$.

State variable	$\overline{\kappa}$				
	0.30	0.35	0.40	0.45	0.50
i_{Le}	20	23.121	27.027	32	38.462
v_{Ce}	280	300.58	324.324	352	384.6154
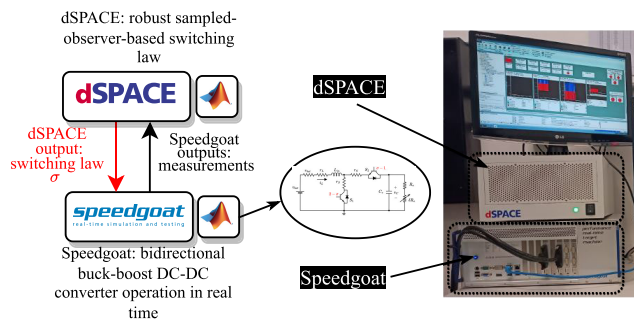
FIGURE 3. HIL experimental setup. The converter circuit is presented in Figure 2.

Furthermore, for practical application purposes, the switching law $\sigma(\hat{\xi}_k)$ in (9) is implemented as follows[5]

$$\sigma(\hat{\xi}_k) = \begin{cases} 1, & \text{if } (\hat{\xi}_k' P((A_1 - A_2)\hat{\xi}_k + (g_1 - g_2)) \leq 0 \\ 2, & \text{if } (\hat{\xi}_k' P((A_1 - A_2)\hat{\xi}_k + (g_1 - g_2)) > 0. \end{cases}$$
(53)

In addition, to validate the efficacy of the strategy, we included a current sensor to measure i_L and a redundant fault-free sensor to measure the output voltage v_C, in order to obtain the system state in real-time during the experiment. Still, we remark that for the observer-based strategy, we only consider fault-prone voltage sensors.

B. PERFORMANCE UNDER DIFFERENT SCENARIOS
To illustrate the performance of the proposed approach, five different scenarios were tested using a hardware-in-the-loop (HIL) experimental platform. As shown in Figure 3, the bidirectional buck-boost DC–DC converter was implemented in Speedgoat™, while the proposed strategy was implemented in dSPACE™. The characteristics of each scenario are described in Table 4, whereas Figure 4 shows the change in the equilibrium point (see Fig. 4(a)), the uncertainties in the resistance load (see Fig. 4(b)) and the fault signal inserted in the voltage sensor (see Fig. 4(c)). The sensor fault is given by a sinusoidal function $f_s(t) = \beta_f \sin(2\pi t)$ and can be used to represent an injection attack in the measurement signal.

All the scenarios presented in this paper were obtained by considering $T_{\max}^{-1} = 10$ kHz and $T_{\max}^{-1} = 30$ kHz, in order

---

[5]The new representation presents the same behavior as the one obtained in (9), but the "smaller than" operation is computationally faster than finding the minimum in real-time.

TABLE 4. Scenarios characteristics according to uncertainties, sensor faults, duty cycle, and resistance load.

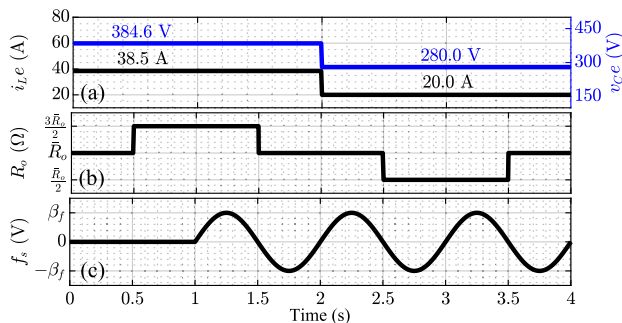| Scenarios	Uncertainties (load R_o)	Sensor faults	Null initial condition
1	x	x	✓
2	✓	x	✓
3	x	✓	✓
4	✓	✓	✓
5	✓	✓	x

FIGURE 4. Events in the converter operation: (a) change in equilibrium point where from $0 \leq t \leq 2s$ the reference is equal to $x_e = [38.462\ 384.615]$. From $t > 2s$, the reference is switched to $[20\ 280]'$, which is equivalent to the equilibrium point when $\overline{\kappa} = 0.30$ (b) load resistance and (c) sensor fault signal, with $\|f_s\| \leq \beta_f = 192.308$ V. The equilibrium inductor current and capacitor voltage are i_{Le} and v_{Ce}, respectively.

to represent the use of switching devices with different switching frequencies. Moreover, for the first four scenarios, we assumed that the capacitor is initially charged at 200 V, whereas in the fifth scenario, the capacitor is completely discharged before the experiment. Thus, when the capacitor is discharged, then $\|x(0) - x_e\| > \omega$, which means that the trajectories of the converter begin outside $\mathcal{B}(x_e, \omega)$.

In the first scenario, the nominal operation of the bidirectional buck-boost DC–DC converter is tested, that is, without uncertainties and sensor faults. The inductor current and capacitor voltage under this scenario are shown in Figure 5. It can be observed that for both values of $T_{\max}$, the current and voltage are maintained close to their reference values. It is important to highlight that the current and voltage errors are not zero due to frequency limitations imposed by the sample time $T_{\max}$. Furthermore, although the dynamic response is similar considering the values of $T_{\max}$, for $T_{\max}^{-1} = 30$ kHz, the state variables are closer to the equilibrium point.

In the second scenario, the converter operation with uncertainties in the resistance load and without sensor faults was analyzed. The inductor current and the capacitor voltage are shown in Figure 6. As the controller is designed for the nominal condition, the uncertainties (variation of the load around $\bar{R}_o$) cause a large deviation from the references for 0.5 s $\leq t \leq 1.5$ s and 2.5 s $\leq t \leq 3.5$ s. Furthermore, the maximum deviation from the reference (worst performance) is obtained for the second equilibrium point once the controller is designed for the first one x_e.

In the third scenario, the effect of sensor faults was analyzed without considering uncertainties in the load resistance.
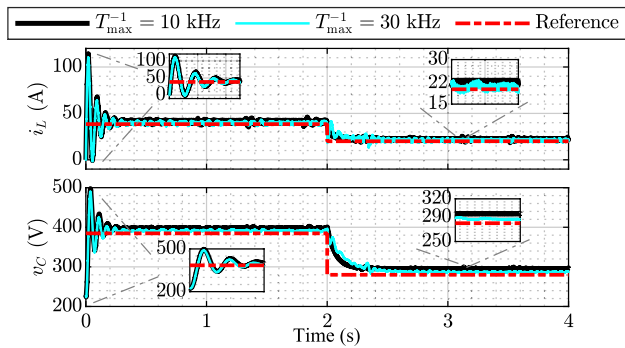
FIGURE 5. Scenario 1: inductor current i_L and capacitor voltage v_C considering operation without uncertainties and without sensor faults for different values of $T_{\max}$ and a change in the equilibrium point.
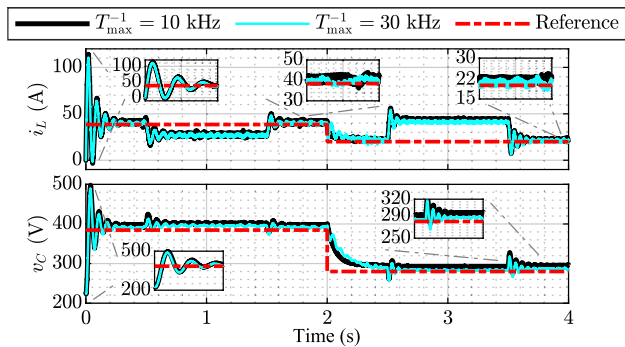

FIGURE 6. Scenario 2: inductor current i_L and capacitor voltage v_C considering operation with uncertainties on the load resistance and without sensor faults, considering different values of $T_{\max}$ and a change in the equilibrium point.
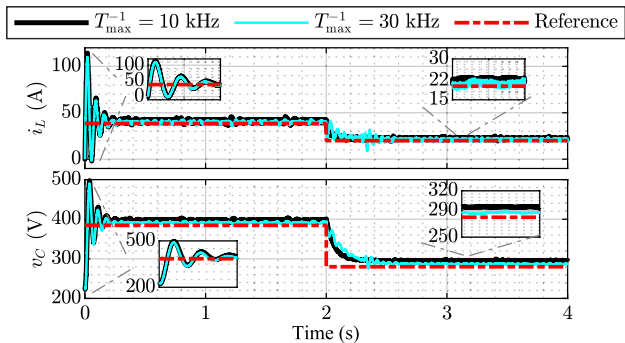

FIGURE 7. Scenario 3: inductor current i_L and capacitor voltage v_C considering operation without uncertainties and with sensor faults considering different values of $T_{\max}$ and a change in the equilibrium point.

As shown in Figure 7, the state variables are controlled close to the equilibrium points, even with a sinusoidal false-data injection attack in the sensor measurement. Compared with the second scenario, in which uncertainty in the resistance load is present, the deviation is reduced. The error between the state and the reference is lower when $T_{\max}^{-1} = 30$ kHz.

Finally, in the fourth and fifth scenarios, the effects of sensor faults and uncertainties were analyzed. The capacitor is initially charged in the fourth scenario, as in
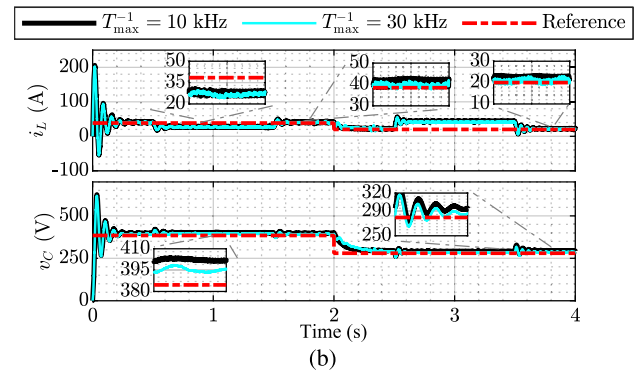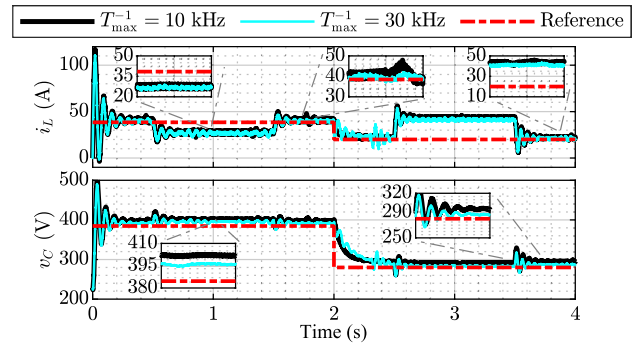

FIGURE 8. Scenarios 4 and 5: Inductor current i_L and capacitor voltage v_C considering operation with uncertainties on the load resistance and with sensor faults for different values of $T_{\max}$ and a change in the equilibrium point. (a) capacitor initially charged in scenario 4 and (b) capacitor initially discharged in scenario 5.

scenarios 1-3, whereas in the fifth scenario, the capacitor was initially discharged. The inductor current and capacitor voltage for both conditions are shown in Figure 8, considering two values of $T_{\max}$. As can be seen, the state variable is controlled around the reference even under uncertainties in the resistance load and when the sensor is under a false-data injection attack at $t = 2$ s. On the other hand, when the capacitor is initially charged (see Fig. 8(a)), the current and voltage overshoot are lower than when the capacitor is initially discharged (see Fig. 8(b)). This shows that by applying the switching law in (9), the bidirectional buck-boost converter is under more stress when the initial condition is null, which can be dangerous for most practical applications.

We remark that in the fourth and fifth scenarios, we aimed to obtain the maximum deviation from the equilibrium point for the worst-case scenario considered in Theorem 2, when system (1) is under uncertainties, sensor faults, and change in the equilibrium points. In the fifth scenario, we obtained the trajectories of the converter when $\|x(0) - x_e\| > \omega$. The phase plane for the fifth scenario is shown in Figure 9. As the initial condition is null, the trajectory starts outside the green ball of radius $\omega = 184.796$, calculated according to (8), until it reaches the red ball of radius $\omega_E \approx 119$, which is an approximation of the experimental attraction region, defined as $\mathcal{B}(x_e, \omega_E)$. Once the trajectory is inside the ball $\mathcal{B}(x_e, \omega)$, it is maintained there for all time, as stated by Theorem 1. In the zoomed regions, it is possible to see that the current and voltage errors are not null but limited.
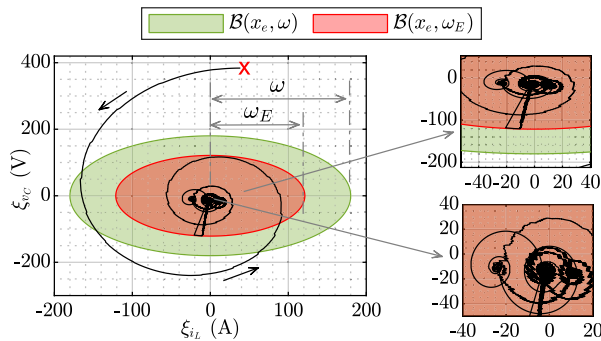
FIGURE 9. Experimental phase plane for scenario 5. The green ball represents the theoretical attraction region calculated in (8), while the red ball represents an approximation to the experimental attraction region.
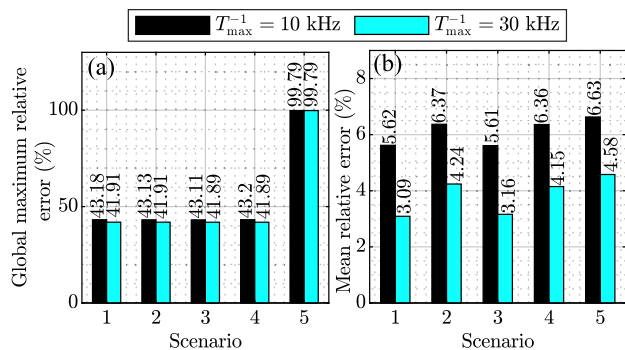

FIGURE 10. Performance index for all scenarios considering different values of T_{max}: (a) global maximum relative error (GMRE) and (b) mean relative error (MRE).

To mathematically analyze the performance of the proposed strategy under the four scenarios and for both values of T_{max}, the global maximum relative error (GMRE) and mean relative error (MRE) were evaluated as follows:

$$\text{MRE (\%)} = \frac{100\%}{N} \sum_{z=1}^{N} \frac{\|x[z] - x_e[z]\|}{\|x_e[z]\|} \tag{54}$$

$$\text{GMRE (\%)} = 100\% \max_{z=1\cdots N} \left(\frac{\|x[z] - x_e[z]\|}{\|x_e[z]\|} \right) \tag{55}$$

where z is the index for the signal samples and N is the total number of samples. The errors for all the scenarios are shown in Figure 10. It can be observed that in scenario 5, the errors are the largest due to the fact that the converter has a null initial condition, which implies large initial errors. Furthermore, in relation to the values of T_{max}, the errors in all scenarios were larger considering $T_{max}^{-1} = 10$ kHz.

VI. CONCLUDING REMARKS AND FUTURE DIRECTIONS
We provided a method to obtain a switching law and observer gains to guarantee fault tolerance against bounded sensor faults and robustness against norm-bounded uncertainties, where all gains are a solution to an optimization problem that guarantees the smallest region of attraction within the given upper bounds $\overline{\alpha}_i$ in (41), by solving (38) in Theorem 2. Theorem 1 provides a more realistic approximation of the radius to which the trajectories of the uncertain switched

affine system are attracted. The proposed strategy offers enhanced reliability in the presence of sensor faults and uncertainties, making it a valuable tool for real-world applications in control systems, particularly when not all state variables are available for measurement.

Moreover, we considered the frequency limitations of switching devices by setting two different sample times, showing that the gains obtained in Theorem 2 are sufficient to guarantee the practical stability of DC–DC bidirectional buck-boost converters for switching frequencies greater than 10 kHZ, which allows the application of the strategy for different switching devices, without the need to update the gain matrices. Furthermore, using Algorithm 2, we also showed that the observer gains and switching law obtained guarantee the practical stability of the switched system for a range of equilibrium points instead of only one, which can be a valuable result in a practical scenario. In addition, the experiments showed that stability is guaranteed under norm-bounded uncertainties even if all sensors are faulty with a maximum relative error of 6.63% in the worst-case scenario.

In future works, a sliding-mode observer-based strategy or data-driven-based methods will be considered to obtain improved state estimation. Additionally, component faults, disturbances, and uncertainties in the b_i matrices in (1) are issues of interest to be addressed with sampled-based switching. In addition, the proposed strategy can be applied to DC–DC converters with more complex topologies. Furthermore, heuristic methods can be applied to obtain a better estimation of the region of attraction ω in Theorem 3 considering different parameters η and $\overline{\alpha}_i$ in Theorem 2. Also, Algorithm 2 can be improved to find more equilibrium points using the same observer and switching law matrices obtained in Theorem 2.

REFERENCES
[1] E. Effah and O. Thiare, "Survey: Faults, fault detection and fault tolerance techniques in wireless sensor networks," *Int. J. Comput. Sci. Inf. Secur.*, vol. 16, no. 10, pp. 1–14, Oct. 2018.

[2] M. Mola, N. Meskin, K. Khorasani, and A. Massoud, "Distributed event-triggered consensus-based control of DC microgrids in presence of DoS cyber attacks," *IEEE Access*, vol. 9, pp. 54009–54021, 2021.

[3] M. Ghiasi, M. Dehghani, T. Niknam, A. Kavousi-Fard, P. Siano, and H. H. Alhelou, "Cyber-attack detection and cyber-security enhancement in smart DC-microgrid based on blockchain technology and Hilbert Huang transform," *IEEE Access*, vol. 9, pp. 29429–29440, 2021.

[4] V. L. Yoshimura, E. Assunção, E. R. P. da Silva, M. C. M. Teixeira, and E. I. M. Júnior, "Observer-based control design for switched affine systems and applications to DC–DC converters," *J. Control, Autom. Electr. Syst.*, vol. 24, no. 4, pp. 535–543, Aug. 2013.

[5] M. Xiao, G. Zhai, and C. Huang, "Quadratic stabilisation of switched affine systems," *J. Control Decis.*, vol. 7, no. 1, pp. 1–23, Jan. 2020.

[6] H. Xie, G. Zong, D. Yang, Y. Chen, and K. Shi, "Dynamic output feedback $\mathcal{L}_\infty$ control of switched affine systems: An event-triggered mechanism," *Nonlinear Anal., Hybrid Syst.*, vol. 47, Feb. 2022, Art. no. 101278.

[7] G. S. Deaecto, "Dynamic output feedback $\mathcal{H}_\infty$ control of continuous-time switched affine systems," *Automatica*, vol. 71, pp. 44–49, Sep. 2016.

[8] H. Xie, G. Zong, D. Yang, and K. Shi, "Input-to-state practical stability analysis and controller design of switched affine systems: An observer-based approach," *Asian J. Control*, vol. 25, no. 4, pp. 3045–3056, Jul. 2023.

[9] J. Li, Z. Zhang, and B. Li, "Sensor fault detection and system reconfiguration for DC–DC boost converter," *Sensors*, vol. 18, no. 5, p. 1375, Apr. 2018.

[10] D. S. Carneiro, L. J. R. Silva, F. A. Faria, R. F. Q. Magossi, and V. A. Oliveira, "Reconfiguration strategy for a DC–DC boost converter using sliding mode observers and fault identification with a neural network," in *Proc. Procedings do XV Simpósio Brasileiro de Automação Inteligente*, 2021, pp. 1338–1344.

[11] M. A. Rezaei, A. Fathollahi, S. Rezaei, J. Hu, M. Gheisarnejad, A. R. Teimouri, R. Rituraj, A. H. Mosavi, and M.-H. Khooban, "Adaptation of a real-time deep learning approach with an analog fault detection technique for reliability forecasting of capacitor banks used in mobile vehicles," *IEEE Access*, vol. 10, pp. 132271–132287, 2022.

[12] M. A. Rezaei et al., "Reliability calculation improvement of electrolytic capacitor banks used in energy stothe set composed of the first M positive integers is denoted as M, where M is the number of system modesrage applications based on internal capacitor faults and degradation," *IEEE Access*, vol. 12, pp. 13146–13164, 2024, doi: 10.1109/ACCESS.2024.3351604.

[13] J.-D. Lee, D.-H. Park, and R.-Y. Kim, "Novel variable switching frequency PWM strategy for a SiC-MOSFET-based electric vehicle inverter to increase battery usage time," *IEEE Access*, vol. 10, pp. 21929–21940, 2022.

[14] L.-L. Li, J. Zhao, and G. M. Dimirovski, "Multiple Lyapunov functions approach to observer-based $\mathcal{H}_\infty$ control for switched systems," *Int. J. Syst. Sci.*, vol. 44, no. 5, pp. 812–819, 2013.

[15] L. I. Allerhand and U. Shaked, "Robust state-dependent switching of linear systems with dwell time," *IEEE Trans. Autom. Control*, vol. 58, no. 4, pp. 994–1001, Apr. 2013.

[16] C. A. Sanchez, G. Garcia, S. Hadjeras, W. P. M. H. Heemels, and L. Zaccarian, "Practical stabilization of switched affine systems with dwell-time guarantees," *IEEE Trans. Autom. Control*, vol. 64, no. 11, pp. 4811–4817, Nov. 2019.

[17] A. Russo, G. P. Incremona, A. Cavallo, and P. Colaneri, "State dependent switching control of affine linear systems with dwell time: Application to power converters," in *Proc. Amer. Control Conf. (ACC)*, Jun. 2022, pp. 3807–3813.

[18] J. C. Geromel and P. Colaneri, "Stability and stabilization of continuous-time switched linear systems," *SIAM J. Control Optim.*, vol. 45, no. 5, pp. 1915–1930, 2006.

[19] M. A. Müller and D. Liberzon, "Input/output-to-state stability of switched nonlinear systems," in *Proc. Amer. Control Conf.*, Jun. 2010, pp. 1708–1712.

[20] S. Veer and I. Poulakakis, "Switched systems with multiple equilibria under disturbances: Boundedness and practical stability," *IEEE Trans. Autom. Control*, vol. 65, no. 6, pp. 2371–2386, Jun. 2020.

[21] R. Wang, L. Hou, G. Zong, S. Fei, and D. Yang, "Stability and stabilization of continuous-time switched systems: A multiple discontinuous convex Lyapunov function approach," *Int. J. Robust Nonlinear Control*, vol. 29, no. 5, pp. 1499–1514, Mar. 2019.

[22] S. Zhuo, L. Xu, A. Gaillard, Y. Huangfu, D. Paire, and F. Gao, "Robust open-circuit fault diagnosis of multi-phase floating interleaved DC–DC boost converter based on sliding mode observer," *IEEE Trans. Transport. Electrific.*, vol. 5, no. 3, pp. 638–649, Sep. 2019.

[23] X. Xiao and L. Zhou, "Mode-dependent IOSS conditions for continuous-time switched nonlinear systems," *Int. J. Control, Autom. Syst.*, vol. 19, no. 11, pp. 3580–3587, Nov. 2021.

[24] C. A. Sanchez, A. Ventosa-Cutillas, A. Seuret, and F. Gordillo, "Robust switching control design for uncertain discrete-time switched affine systems," *Int. J. Robust Nonlinear Control*, vol. 30, no. 17, pp. 7089–7102, Nov. 2020.

[25] G. S. Deaecto and L. N. Egidio, "Practical stability of discrete-time switched affine systems," in *Proc. Eur. Control Conf. (ECC)*, Jun. 2016, pp. 2048–2053.

[26] L. N. Egidio and G. S. Deaecto, "Novel practical stability conditions for discrete-time switched affine systems," *IEEE Trans. Autom. Control*, vol. 64, no. 11, pp. 4705–4710, Nov. 2019.

[27] L. Hetel and E. Fridman, "Robust sampled—Data control of switched affine systems," *IEEE Trans. Autom. Control*, vol. 58, no. 11, pp. 2922–2928, Nov. 2013.

[28] Z. Li, D. Ma, and J. Zhao, "Dynamic event-triggered $\mathcal{L}_\infty$ control for switched affine systems with sampled-data switching," *Nonlinear Anal., Hybrid Syst.*, vol. 39, Feb. 2021, Art. no. 100978.

[29] L. Zhang, X. Lou, and Z. Wang, "Output-based robust switching rule design for uncertain switched affine systems: Application to DC–DC converters," *IEEE Trans. Circuits Syst. II, Exp. Briefs*, vol. 69, no. 11, pp. 4493–4497, Nov. 2022.

[30] I. R. Petersen, "A stabilization algorithm for a class of uncertain linear systems," *Syst. Control Lett.*, vol. 8, no. 4, pp. 351–357, Mar. 1987.

[31] T. J. Meijer, T. Holicki, S. J. A. M. van den Eijnden, C. W. Scherer, and W. P. M. H. Heemels, "The non-strict projection lemma," *IEEE Trans. Autom. Control*, early access, 2024, doi: 10.1109/TAC.2024.3371374.

[32] L. J. Elias, F. A. Faria, R. Araujo, R. F. Magossi, and V. A. Oliveira, "Robust static output feedback $\mathcal{H}_\infty$ control for uncertain fuzzy systems," *IEEE Trans. Fuzzy Syst.*, vol. 30, no. 10, pp. 4434–4446, Oct. 2022.

[33] R. Piziak and P. L. Odell, "Full rank factorization of matrices," *Math. Mag.*, vol. 72, no. 3, pp. 193–201, Jun. 1999.

DIEGO DOS SANTOS CARNEIRO received the B.Eng. degree in control and automation engineering from the Federal University of Ouro Preto, Brazil, in 2019. He is currently pursuing the Ph.D. degree with the Universidade de São Paulo, São Paulo, Brazil. He was a Visiting Ph.D. Student at the University of Pavia, Pavia, Italy, from May 2022 to February 2023. He is currently a Research and Development Developer at XMobots Aerospace and Defense, Brazil. His research interests include fault detection, isolation, and reconfiguration for uncertain switched affine systems.
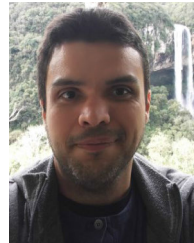
FLÁVIO ANDRADE FARIA received the B.Math., M.Sc., and Ph.D. degrees in electrical engineering from São Paulo State University (UNESP), in 2003, 2005, and 2009, respectively. Since 2013, he has been an Assistant Professor with UNESP. His research interests include linear-matrix-inequality-based control designs, Takagiâ-Sugeno fuzzy modeling, and its applications.
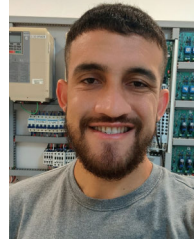
LUCAS JONYS RIBEIRO SILVA was born in Viçosa, Brazil, in 1997. He received the B.S. degree in electrical engineering from the Federal University of Viçosa, in 2020, and the M.S. degree from the Universidade de São Paulo, in 2022, where he is currently pursuing the Ph.D. degree in electrical engineering. His main research interests are in the fields of microgrids, electric and hybrid vehicles, energy management, and dc/dc converters for renewable energy sources and storage systems.

BRUNO MENEGHEL ZILLI was born in Medianeira, Brazil. He received the B.S. degree in electronic engineering from the Federal University of Technology-Paraná, in 2015, and the M.S. degree in energy in agriculture engineering from Western Paraná State University, in 2018. He is currently pursuing the Ph.D. degree in electrical engineering with the Universidade de São Paulo. His main research interests are in the fields of microgrids, harmonic compensation, energy management, and renewable energy sources.

VILMA ALVES DE OLIVEIRA (Life Senior Member, IEEE) received the B.Eng. degree in electronics from the Universidade do Estado do Rio de Janeiro, Rio de Janeiro, Brazil, in 1976, the M.Sc. degree from the Universidade Federal do Rio de Janeiro, Rio de Janeiro, in 1980, and the Ph.D. degree from the University of Southampton, Southampton, U.K., in 1989, both in electrical engineering. In 1990, she joined the Department of Electrical and Computing Engineering, Universidade de São Paulo, São Paulo, Brazil, where she is currently a Full Professor. Her research interests include fuzzy control and control design and their applications. She is currently the Editor-in-Chief of *Journal of Control, Automation and Electrical Systems*.

● ● ●